Energy Conversion and Management 127 (2016) 526–544

Contents lists available at ScienceDirect

Energy Conversion and Management

journal homepage: www.elsevier.com/locate/enconman

NLP modeling for the optimization of LiBr-H_2O absorption refrigeration systems with exergy loss rate, heat transfer area, and cost as single objective functions

Sergio F. Mussati [a,b], Krist V. Gernaey [c], Tatiana Morosuk [d], Miguel C. Mussati [a,b,*]

[a] INGAR Instituto de Desarrollo y Diseño (CONICET-UTN), Avellaneda 3657, S3002GJC Santa Fe, Argentina
[b] CAIMI Centro de Aplicaciones Informáticas y Modelado en Ingeniería, Facultad Regional Rosario, Universidad Tecnológica Nacional, Zeballos 1341, S2000BQA Rosario, Argentina
[c] CAPEC-PROCESS Research Center, Department of Chemical and Biochemical Engineering, Technical University of Denmark (DTU), Søltofts Plads, Building 229, DK-2800 Kgs. Lyngby, Denmark
[d] Technische Universität Berlin, Institute for Energy Engineering, Marchstr. 18, 10587 Berlin, Germany

ARTICLE INFO

Article history:
Received 17 May 2016
Received in revised form 3 September 2016
Accepted 6 September 2016
Available online 19 September 2016

Keywords:
Absorption refrigeration systems
LiBr–H_2O
Optimal area distribution
Exergy loss minimization
Cost minimization
NLP modeling
GAMS

ABSTRACT

Based on a nonlinear mathematical programming model, the sizes and operating conditions of the process units of single-effect absorption refrigeration systems operating with a LiBr–H_2O solution are optimized for a specified cooling capacity by minimizing three single objective functions: the total exergy loss rate, the total heat transfer area, and the total annual cost of the system.

It was found that the optimal solution obtained by minimization of the total exergy loss rate provides "theoretical" upper bounds not only for the total heat transfer area of the system but also for each process unit and all stream temperatures, while the optimal solution obtained by minimization of the total heat transfer area provides the lower bounds for these model variables, to solve a cost optimization problem.

The minimization of the total exergy loss rate by varying parametrically the available total heat transfer area between these bounds was also performed, allowing to see how the optimal distribution of the available total heat transfer area among the system components, as well as the operating conditions (stream temperature, pressure, composition, and mass flow rate) and heat loads, vary qualitatively and quantitatively with increasing available total heat transfer area. These optimization results allowed to find a "practical" value of the total heat transfer area, i.e. no benefits can be obtained by increasing the available total heat transfer area above this value since the minimal total exergy loss value cannot be significantly improved by distributing additional heat transfer area among the process units. The optimal solution corresponding to this practical value significantly improves the upper bounds for an economic optimization problem with respect to the optimal solution corresponding to the theoretical value.

The optimal solutions corresponding to the theoretical and the practical upper bound values for the total heat transfer area (100 m^2 and 61 m^2, respectively) as well as the optimal solution obtained by minimization of the total annual cost are discussed for a case study considering a cooling capacity of 50 kW, upon the model assumptions made and a given cost model. Around three-quarters of the minimal total annual cost correspond to capital expenditures and the rest to operating expenditures. The generator and evaporator represent together around 70% of the capital expenditures. The absorber is the largest contributor to both the total heat transfer area and the total exergy loss rate, with around 33.19 and 39.16%, respectively, when the total annual cost is minimized.

1. Introduction

Different methodologies have been proposed and applied to accomplish the challenge of improving absorption refrigeration systems (ARSs). Indeed, many works dealing with the study of ARSs based on the second law of thermodynamics (exergy and exergoeconomic analyses) and mathematical programming have been published. Exergy analysis is widely applied to evaluate the

* Corresponding author at: INGAR Instituto de Desarrollo y Diseño (CONICET-UTN), Avellaneda 3657, S3002GJC Santa Fe, Argentina.
E-mail addresses: mussati@santafe-conicet.gov (S.F. Mussati), kvg@kt.dtu.dk (K.V. Gernaey), tetyana.morozyuk@tu-berlin.de (T. Morosuk), mmussati@santafe-conicet.gov.ar (M.C. Mussati).

http://dx.doi.org/10.1016/j.enconman.2016.09.021
0196-8904/

Nomenclature

A_k	cost parameter for estimating investment for a process unit k (Eq. (26))
b_i	specific exergy of a process stream i (kJ kg^{-1})
B_i	exergy flow rate of a process stream i (kW)
B_k	cost parameter for estimating investment for a process unit k (Eq. (26))
C_k	cost parameter for estimating investment for a process unit k (Eq. (26))
$CAPEX$	capital expenditures (\$ yr^{-1})
CRF	capital recovery factor (dimensionless)
CU	cooling utility (tn yr^{-1})
$E_{L,tot}$	total exergy loss rate of the system (kW)
$E_{L,k}$	exergy loss rate in process unit k (kW)
$\mathbf{g}_t$	set of inequality constraints t
$\mathbf{h}_s$	set of equality constraints s
h_i	specific enthalpy of a process stream i (kJ kg^{-1})
H_i	enthalpy flow rate of a process stream i (kW)
HTA_k	heat transfer area of a process unit k (m^2)
HU	heating utility (tn yr^{-1})
i	interest rate (dimensionless)
IN	subset of PS with the streams i entering a process unit k, except for utility streams (cooling water, chilled water, and hot water)
$LMTD_k$	logarithmic mean temperature difference in a process unit k
M_i	mass flow rate of a process stream i (kg s^{-1})
n	project lifetime (yr)
$OPEX$	operating expenditures (\$ yr^{-1})
OUT	subset of PS with the streams i leaving a process unit k, except for utility streams (cooling water, chilled water, and hot water)
p_{THTA}	a model parameter that refers a fixed value of THTA (m^2)
P	pressure (kPa)
PC	set of the system components j
PS	set of the process streams i
PU	set of the process units k
Q_k	heat load in a process unit k; exchanged heat (kW)
S	entropy (J K^{-1})
T_i	temperature of a stream i (°C, K)
TAC	total annual cost (\$ yr^{-1})
$THTA$	total heat transfer area of the system (m^2)
U_k	overall heat transfer coefficient for process unit k (kW m^{-2} °C^{-1})
W_k	power in a process unit k (kW)
$\mathbf{x}$	vector of model variables
X_j	mass fraction of component j (kg kg^{-1})
Z_k	investment for a process unit k (\$ yr^{-1})

Greek letters

Δ	refers to the difference between two values
η	effectiveness of the solution heat exchanger SHE (dimensionless)

Abbreviations

ABS	absorber
COND	condenser
COND1	condenser for sensible heat
COND2	condenser for latent vaporization heat
CU	cooling utility
EV	expansion valve
EVAP	evaporator
GEN	generator

Acronyms

ARS	absorption refrigeration system
COP	coefficient of performance
CPU	central processing unit
GA	genetic algorithms
GAMS	General Algebraic Modeling System
HTA	heat transfer area
HU	heating utility
LCA	life cycle assessment
LMTD	logarithmic mean temperature difference
MILP	mixed-integer linear programming
MINLP	mixed integer nonlinear programming
moMINLP	multi-objective mixed integer nonlinear programming
NLP	nonlinear programming
OP	optimization problem
SA	simulated annealing
SHE	solution heat exchanger
TAC	total annual cost
THTA	total heat transfer area

Subscripts

CU	cooling utility
HU	heating utility
i	a process stream
in	inlet
j	a system component
k	a process unit
L	loss
min	minimum
out	outlet
s	an equality constraint of the mathematical optimization model
t	an inequality constraint of the mathematical optimization model
tot	total
u	utility (cooling water, chilled water, and hot water)

Superscripts

C	cold side of a heat exchanger
H	hot side of a heat exchanger

thermal efficiency level of a system, and to identify the most inefficient system components. Special attention should then be focused on such components to minimize the irreversible losses.

Morosuk and Tsatsaronis [1,2] have developed an approach to perform an exergy analysis of absorption and vapor-compression refrigeration systems in a more advanced way, which consists of splitting the exergy destruction within each process unit into endogenous/exogenous and unavoidable/avoidable parts, followed by identifying the potential to improve each one. These splits improve the accuracy of exergy analysis and the understanding of the thermodynamic inefficiencies, and facilitate an exergoeconomic optimization. Cai et al. [3] presented a methodology of exergy analysis for NH_3–$LiNO_3$ and NH_3–NaSCN absorption refrigeration cycles considering a novel air-cooled type non-adiabatic absorber to improve both the coefficient of performance (COP) and the exergetic efficiency of the system under air cooling

conditions. They highlighted that non-adiabatic absorbers significantly increase the system exergetic efficiency, and that for low evaporating temperature conditions, non-adiabatic absorbers are absolutely necessary for air-cooled type NH_3–NaSCN and NH_3–$LiNO_3$ systems. Kaynakli et al. [4] developed and coded in Delphi a simulation model to perform energy and exergy analyses of a double-effect series-flow ARS with H_2O–LiBr as working fluid pair. They studied parametrically the effect of the operation temperatures of the whole system (generators, evaporator, absorber, and condenser) on the exergy destruction of the high pressure generator, COP of the system, and mass flow rate when different heat sources are employed (hot water, hot air, and steam). The results comparison showed that the hot air leads to the maximum exergy destruction value, followed by steam and hot water.

On the other hand, thermoeconomics, also called exergoeconomics, is another alternative and useful tool for seeking improvement of thermal systems which combines the thermodynamic analysis with principles of economics. The thermoeconomic cost balance is formulated in the same way as the exergy balance but including the investment and operating and maintenance costs of the entire process. Exergoeconomic methods may be grouped in algebraic methods and calculus methods [5,6]. The algebraic methods use algebraic balance equations, and require the proposal of auxiliary cost equations for each component, which is a subjective task. On the other hand, the calculus methods use differential equations, where the system cost flows are obtained in conjunction with optimization procedures based on the method of Lagrange multipliers, which determines marginal costs. In the calculus methods, the mathematical description of the function of each component is also subjective.

Misra et al. [7] applied thermoeconomic evaluation and optimization to double-effect LiBr–H_2O ARSs. They concluded that the thermoeconomic analysis of a system is able to provide suggestions about potential cost-effective improvements, achievable by means of changes in the values of the internal operating parameters of the system. Farshi et al. [8] investigated the influence of various operating parameters on the total cost of the whole system for three configurations of double-effect H_2O–LiBr ARSs (series, parallel, and reverse parallel systems). They considered the dependence of the heat transfer coefficients on the operating conditions for designing the heat exchangers. The contributions of component costs to the overall costs were obtained for each system, and the results of the exergoeconomic analyses of the systems were described. Mosaffa et al. [9] presented exergoeconomic and environmental analyses for two CO_2–NH_3 cascade refrigeration systems. One system includes two flash tanks and the other one includes a flash tank along with a flash intercooler with indirect subcooler. By using the EES- Engineering Equation Software and parametric simulations, they obtained the values of system operating parameters that maximize the COP and exergy efficiency and minimize the total annual cost.

In general, the methods based on exergy analysis imply an iterative process, where all the process units are considered in thermoeconomic isolation; this means that the efficiency-related variables of a given unit are analyzed independently of the remaining units and they are allowed to change, while the variables of the other units are kept constant [10]. Then, depending on the degrees of freedom of the optimization problem (number of variables minus number of equality constraints), the exergy-based methods may require a considerable number of iterations and calculations to be applied [11], and even more if optimization studies are performed. In addition, the consideration of the isolation principle may imply that only a subset of the possible design solutions is being considered [10]. These two aspects are the main weaknesses of the exergy-based analyses.

On the other hand, systematic methods based on mathematical programming techniques have also been applied to the optimization of refrigeration systems. Unlike the exergy-based optimization approaches, the main advantage of using the mathematical programming techniques is that they allow to simultaneously optimize all the trade-offs existing among the process variables. However, only few publications have dealt with mathematical programming approaches applied to the optimization of energy conversion systems despite of the fact that the performance of the solvers handling nonlinear constraints was greatly improved. Chavez-Islas and Heard [12,13] applied mixed integer nonlinear programming (MINLP) techniques for the optimization of NH_3–H_2O ARSs. They developed a model that includes discontinuous functions for estimating the capital cost of the main system components. The simultaneous optimization of six decision variables (the reflux ratio, the temperature values in the absorber, condenser, subcooler, and reboiler, and the economizer effectiveness) was performed in order to minimize the total annualized cost. The proposed model was applied to two types of heat rejection media: cooling water and air. A result indicated that the selection of the cooling medium is dependent on the required refrigeration level. In addition, the influence of the design variables on the objective function depends strongly on the heat rejection medium type (air or water) and the process requirements (refrigeration level). Rubio-Maya et al. [14] developed a nonlinear programming (NLP) model to minimize the annual operating cost of LiBr–H_2O ARSs considering the temperatures of the generator, condenser, evaporator, and absorber, and the effectiveness of the solution heat exchanger as decision variables. The outlet cooling water temperatures in the condenser and absorber and the outlet chilled water temperature in the evaporator are model parameters, i.e. they are fixed for the optimization. Only one case study was presented and no sensitivity analysis was conducted. Mazzei et al. [15] have implemented a NLP model for a single-effect LiBr–H_2O ARS in the optimization software environment GAMS (General Algebraic Modeling System) for optimization purposes. For fixed values of available total heat transfer area, the optimization consisted in determining how the total area is distributed along the process units with the aim of maximizing the COP. Unlike previous studies [14], the outlet cooling water temperatures in the condenser and absorber and the outlet chilled water temperature in the evaporator were handled as optimization variables, instead of model parameters (fixed values), thus increasing the degrees of freedom of the resulting optimization problem.

Also, there have recently been published several articles dealing with the optimization of refrigeration systems considering multi-objective criteria using gradient-based optimization methods and derivative-free based optimization methods (meta-heuristic algorithms) such as simulated annealing and genetic algorithms. Regarding the former methods, Gebreslassie et al. [16] presented a quantitative decision-support tool for the optimal design of environmentally friendly absorption cycles by minimization of the cost and the environmental impact quantified by the Eco-indicator 99 methodology [17], which follows the principles of the life cycle assessment (LCA) methodology [18]. To do this, a bicriteria NLP problem was formulated, whose solution is defined by a set of Pareto points that represent the optimal trade-off between the considered economic and environmental concerns. Brunet et al. [19] optimized a NH_3–H_2O absorption cycle for cooling and refrigeration applications with economic and environmental concerns, proposing an approach that combines the capabilities of process simulation, multi-objective optimization, cost analysis, and LCA. The optimization task was posed in mathematical terms as a multi-objective mixed-integer nonlinear programming (moMINLP) problem, which was solved by an outer-approximation strategy that iterates between primal NLP sub-problems with fixed binary

variables and a tailored mixed-integer linear programming (MILP) model.

Regarding multi-objective optimization using derivate-free methods, Sayyaadi et al. [20] proposed the optimization of a cooling tower assisted vapor compression refrigeration machine considering simultaneously the system total exergy destruction (as a thermodynamic criterion) and the system total product cost (as an economic criterion). To this end, a thermodynamic model based on energy and exergy analyses and an economic model based on the total revenue requirement (TRR) method were developed. Jain et al. [21] optimized the performance of a 170 kW vapor compression–absorption cascaded refrigeration system based on combined thermodynamic, economic, and environmental parameters, using the non-dominated sort genetic algorithm-II (NSGA-II) technique. The total irreversibility rate and the total cost of the system were the two objective functions considered simultaneously in the multi-objective optimization problem. In both papers [20,21], it was concluded that the multi-objective optimized design is better than the two individual single-objective optimized designs.

Compared to the gradient-based optimization methods, the meta-heuristic algorithms (simulated annealing SA and genetic algorithms GA) are inherently sequential, derivative-free, and well suited for highly complex problems with discontinuous functions and without any known sophisticated solution techniques like the combinatorial optimization problems. The solutions obtained by the two algorithms are strongly dependent on the required parameters; for instance, in GA, on the number of generations, population, crossover rate, mutation rate, and tournament size (number of individuals needed to fill a tournament during selection). They can be usefully applied, for example, in control problems or in highly combinatorial problems (e.g. scheduling problems with many tasks and machines), where the deterministic algorithms may require prohibitively long computing times to obtain optimal solutions. However, if process design and operating conditions are to be optimized without involving controllability and flexibility issues, the deterministic optimization methods (gradient-based methods) are more preferred than SA and GA algorithms.

The research presented in this paper is a continuation of the research presented in [15]. The equation-oriented optimization mathematical model, formulated as a NLP problem, of a single-effect absorption refrigeration system operating with a LiBr–H_2O solution presented in [15] has been extended to perform exergy-based process analysis and optimization. The major contribution of the extended version of the model is that it allows elucidating and simultaneously optimizing the trade-offs that exist among the operating conditions and the size (heat transfer area) of each process unit when the total exergy loss is minimized, instead of pursuing the maximization of the coefficient of performance (COP) as addressed in [15]. Then, because of the NLP type formulation, the resulting deterministic model is able to simultaneously predict the optimal temperature, pressure, mass flow rate, and composition values of each process stream as well as the optimal distribution of the total available heat transfer area among the involved process units that lead to the minimal values of the total exergy loss, for desired design specifications. The total available heat transfer area is varied parametrically obtaining an optimal solution for each value.

The following four optimization problems are solved and analyzed: (i) minimization of the total exergy loss rate of the system; (ii) minimization of the total heat transfer area of the system; (iii) minimization of the total annual cost (capital and operating expenditures) considering the total heat transfer area as an optimization variable and using the bounds computed in (i) and (ii); and (iv) minimization of the total exergy loss rate of the system for different values of the total available heat transfer area to distribute among the process units, ranging between the optimal values of total area found in (i) and (ii). Based on the results obtained from these optimization problems, a systematic solution procedure is proposed for cost optimization problems. Finally, it should be mentioned that, in the current optimization study, the outlet cooling water temperatures in the condenser and absorber and the outlet chilled water temperature in the evaporator are also treated as optimization (decision) variables. This increases the degrees of freedom of the optimization problem, and thereby, the number of trade-offs that exist among the decision variables in comparison to the majority of the published studies.

2. Description of a single-effect LiBr-H_2O absorption refrigeration system

A schematic of an ARS with LiBr and H_2O as absorbent and refrigerant, respectively, is depicted in Fig. 1. It consists of a generator GEN, an absorber ABS, a condenser COND, an evaporator EVAP, a pump PUMP, expansion valves for the refrigerant EV1 and the solution EV2, and a solution heat exchanger SHE.

In the generator, the LiBr-H_2O solution is heated for vaporizing and separating the refrigerant fluid (H_2O) from the solution. The refrigerant vapor flows to the condenser, where heat is transferred to the cooling water as the refrigerant condenses. Then, the condensed liquid flows through an expansion valve EV1 to the evaporator, where refrigerant is evaporated to produce the cooling effect. The refrigerant vapor is afterwards directed to the absorber, where it is absorbed by the high concentration solution coming from the generator, and transfers heat to the cooling water. Finally, the low concentration solution is pumped through the heat exchanger SHE to the generator. The low and high concentration solutions exchange heat in SHE.

3. Process modeling

The mathematical model used to determine the optimal design and operation conditions includes equality constraints to describe the mass, energy, and exergy balances for the process units, relationships for sizing, and correlations for physicochemical and thermodynamic property estimation of states, as well as inequality constraints to, for instance, establish minimum allowable temperature difference approximations or avoid temperature cross situations in heat exchange. The total exergy losses within the system and the total heat transfer area are the two objective functions that are individually minimized as single-objective optimization formulations.

3.1. Model assumptions

The main assumptions considered in the mathematical model are the following:

- Steady state condition.
- Neither pressure drop nor heat loss is considered in the process units.
- The mechanical work of the pump is not considered in the total energy balance as it is neglected compared with the heat transferred in the other process units.
- The refrigerant leaves the condenser and evaporator at saturation conditions.
- The refrigerant leaves the generator at superheated conditions.
- The weak LiBr solution leaves the absorber at saturation condition.
- The strong LiBr solution leaves the generator at equilibrium at its pressure and temperature.

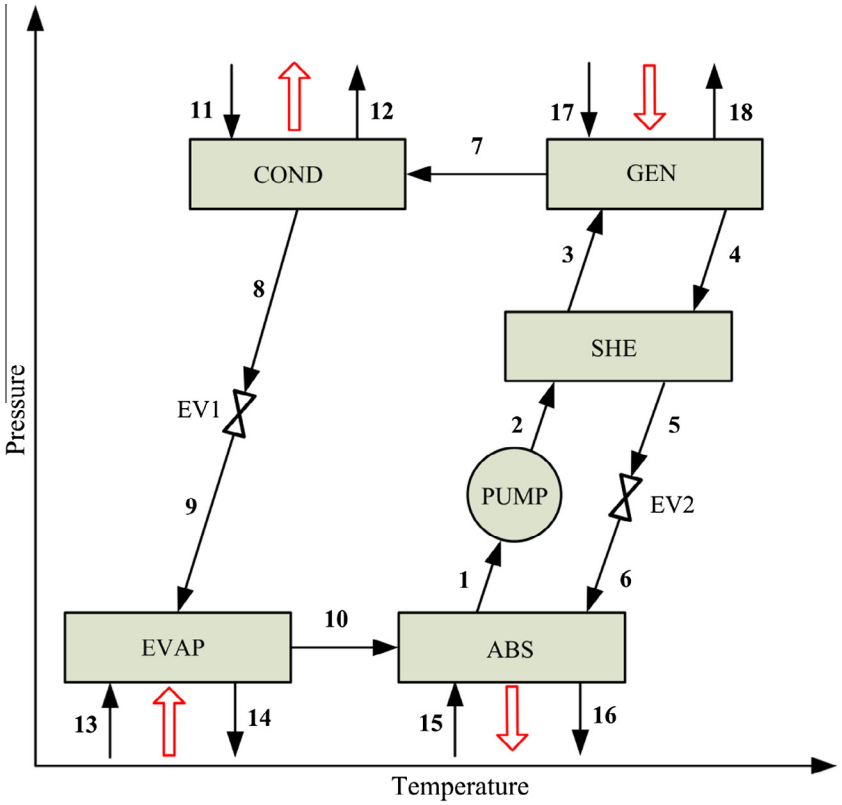

Fig. 1. A schematic representation of a single-effect LiBr-H_2O absorption refrigeration system.

- Dependence of the thermodynamic properties of the LiBr solution on composition and temperature are considered. Similarly, the dependence of water and steam properties on pressure and temperature are considered.
- The expansion valves EV1 and EV2 are included into the exergy balances for the evaporator and absorber, respectively.
- The work of the solution pump is considered negligible.

3.2. Mathematical model formulation

Let *PU* be the set of the main process units *k*:

$$PU = \{ABS, GEN, COND, EVAP, SHE\}$$

Let *PS* be the set of the process streams *i*:

$$PS = \{1, \cdots i \cdots, 18\}$$

Let *PC* be the set of the system components *j*:

$$PC = \{LiBr, water, vapor\}$$

Let *IN* and *OUT* be the subsets of *PS* with the entering and leaving process streams, respectively.

The following balances and relationships can now be formulated according to Fig. 1.

3.2.1. Mass, energy and exergy balances for a process unit k

Total mass balance:

$$\sum_{i\in IN} M_{i,k} - \sum_{i\in OUT} M_{i,k} = 0, \quad \forall k \in PU \tag{1}$$

Component mass balance:

$$\sum_{i\in IN} M_{i,k}\cdot X_{j,i,k} - \sum_{i\in OUT} M_{i,k}\cdot X_{j,i,k} = 0, \quad \forall k \in PU, \quad j = LiBr \tag{2}$$

Energy balance:

$$Q_{u,k} - W_k + \sum_{i\in IN} H_{i,k} - \sum_{i\in OUT} H_{i,k} = 0, \quad \forall k \in PU$$
$$Q_{u,k} = \pm(H_{u,in,k} - H_{u,out,k}) \tag{3}$$

$$H_i = M_i \cdot h_i \tag{4}$$

Exergy balance:

$$E_{L,k} = B_{u,in,k} - B_{u,out,k} + \sum_{i\in IN} B_{i,k} - \sum_{i\in OUT} B_{i,k} = 0, \quad \forall k \in PU \tag{5}$$

$$B_i = M_i \cdot b_i \tag{6}$$

M indicates mass flow rate (kg s^{-1}), *X* refers to mass fraction (kg kg^{-1}), *Q* is the heat load (kW), *W* refers to power (kW), *H* represents enthalpy flow rate (kW), *h* is the specific enthalpy (kJ kg^{-1}), *B* is the exergy flow rate (kW), E_L is the exergy loss rate (kW), and *b* is the specific exergy (kJ kg^{-1}).

The total exergy loss rate $E_{L,tot}$ (kW) is given by:

$$E_{L,tot} = \sum_k E_{L,k}, \quad \forall k \in PU \tag{7}$$

3.2.2. Heat transfer area (HTA) of a process unit k

$$Q_k = U_k \cdot HTA_k \cdot LMTD_k, \quad \forall k \in PU \tag{8}$$

Logarithmic mean temperature difference (LMTD) in process unit k:

$$LMTD_k = \frac{\Delta T_k^H - \Delta T_k^C}{\ln \frac{\Delta T_k^H}{\Delta T_k^C}}, \quad \forall k \in PU \tag{9}$$

where ΔT_k^H and ΔT_k^C are the temperature differences at the hot and cold sides, respectively.

Then, the total heat transfer area *THTA* (m^2) is given by:

$$THTA = \sum_k HTA_k, \quad \forall k \in PU \tag{10}$$

Effectiveness (η) of the solution heat exchanger SHE:

η is based on the strong solution side and it is computed as follows:

$$\eta = \frac{M_3 \cdot \left(H_{3(P_3,T_3,X_3)} - H_{2(P_2,T_2,X_2)}\right)}{M_4 \cdot \left(H_{4(P_4,T_4,X_4)} - H_{2(P_2,T_2,X_2)}\right)} \tag{11}$$

Inequality constraints:

Finally, inequality constraints are included for preventing temperature cross situations. If $\Delta T_{min} = 0.1$ °C is the minimum allowable temperature difference, respectively, the following constraints can be added to the model:Inequality constraints for the solution heat exchanger:

$$T_4 \geqslant T_3 + \Delta T_{min} \tag{12}$$
$$T_5 \geqslant T_2 + \Delta T_{min} \tag{13}$$

Inequality constraints for the condenser:

$$T_7 \geqslant T_{12} + \Delta T_{min} \tag{14}$$
$$T_8 \geqslant T^* + \Delta T_{min} \tag{15}$$
$$T_8 \geqslant T_{11} + \Delta T_{min} \tag{16}$$

Inequality constraints for the generator:

$$T_{17} \geqslant T_7 + \Delta T_{min} \tag{17}$$
$$T_{18} \geqslant T_3 + \Delta T_{min} \tag{18}$$

Inequality constraints for the evaporator:

$$T_{13} \geqslant T_{10} + \Delta T_{min} \tag{19}$$
$$T_{14} \geqslant T_9 + \Delta T_{min} \tag{20}$$

Inequality constraints for the absorber:

$$T_6 \geqslant T_{16} + \Delta T_{min} \tag{21}$$
$$T_1 \geqslant T_{15} + \Delta T_{min} \tag{22}$$

3.2.3. Physicochemical properties estimation

Finally, the model includes correlations to compute the physicochemical properties of the process streams (weak and strong LiBr solutions, water and vapor). The LiBr solution enthalpy in the 40–70% concentration range is estimated by the correlation proposed in [22]. Water and vapor properties are estimated by correlations taken from [23], and the entropy of the process streams was calculated by correlations obtained from [24].

The parameters used for optimization are listed in Table 1. The main decision variables considered for optimization are the temperature, pressure, composition and flow rate of all streams. Lower and upper bounds of the main process variables are listed in Table 2.

Table 1
Process data.

Parameter	Value
Cooling capacity (kW)	50.00
Inlet temperature (°C)	
– Cooling water in the condenser, T_{11}	27.00
– Cooling water in the absorber, T_{15}	30.00
– Chilled water in the evaporator, T_{13}	13.00
– Hot water in the generator, T_{17}	92.00
Heat transfer coefficient (kW m^{-2} $°C^{-1}$)	
– Evaporator, U_{EVAP}	1.50
– Absorber, U_{ABS}	0.70
– Condenser, U_{COND}	2.50
– Generator, U_{GEN}	1.50
– Solution heat exchanger, U_{SHE}	1.00

Table 2
Lower and upper bounds on optimization variables.

Variable	Lower bound	Upper bound
LiBr concentration (%)	40.00	70.00
Pressure (kPa)	0.10	15.00
Mass flow rate of refrigerant and LiBr solutions (kg s^{-1})	0.00	100.00

3.2.4. Cost estimation

The total annual cost (*TAC*) is computed by Eq. (23) in terms of the total capital expenditures (*CAPEX*) and the total operating expenditures (*OPEX*):

$$TAC = CAPEX + OPEX \tag{23}$$

where *CAPEX* is computed by Eq. (24) in terms of the capital recovery factor (*CRF*) and the investment for each process unit k (Z_k), which are computed by Eqs. (25) and (26), respectively. The *CRF* is computed for a project lifetime n of 25 years and an interest rate i of 0.1033.

$$CAPEX = CRF \cdot \sum_k Z_k \tag{24}$$

$$CRF = \frac{i \cdot (1+i)^n}{(1+i)^n - 1} \tag{25}$$

$$Z_k = A_k \cdot HTA_k^{B_k} + C_k \tag{26}$$

The correlation used for estimating Z_k (with A expressed in ft^2) was taken from [25], and the numerical values of parameter A, B, and C are listed in Table 7.

The *OPEX* is computed by Eq. (27), which includes the cost associated with the heating (*HU*) and cooling (*CU*) utilities, whose unitary costs are $C_{HU} = 3.0\$\ tn^{-1}$ and $C_{CU} = 0.0195\$\ tn^{-1}$, respectively.

$$OPEX = C_{HU} \cdot HU + C_{CU} \cdot CU \tag{27}$$

3.3. Computational tools

The resulting NLP problem consisting of 230 equality constraints and 17 inequality constraints was implemented in the General Algebraic Modeling System (GAMS v.23.7) [26] and solved with CONOPT 3.0 [27]. These tools were selected based on past experience in using them to model and optimize a variety of processes and systems of diverse nature, complexity, and size, such as multi-stage flash (MSF) distillation and multi-effect evaporation (MEE) for sea water desalination [28,29], wastewater treatment plants [30,31], azeotrophic batch distillation [32], heat exchangers network for fuel processors for fuel cells [33], combined heat and power plants [34,35], amine-based absorption systems for CO_2 capture [36,37], and more recently, multi-stage membrane systems for CO_2 capture [38]. Some of these applications resulted in NLP models which were efficiently solved using the local optimizer CONOPT supported in GAMS, which is well suited for models with highly nonlinear constraints. It should be noted that CONOPT 3.0 is a local search optimization algorithm based on the generalized reduced gradient method, and therefore, optimal global solutions cannot be theoretically guaranteed due to the presence of nonconvex constraints (mainly bilinear terms in the energy and exergy balances). However, for the wide variation range of the total heat transfer area examined and the sets of values used for problem initialization, no numerical convergence problems were encountered and proper tendencies (curves) of the decision vari-

ables were computed, which is an indication that a good (optimal) solution for each value of total heat transfer area was obtained.

Apart from GAMS, there exist other specific software tools for modeling and optimization of nonlinear systems such as AIMMS–Advanced Integrated Multidimensional Modeling Software [39], AMPL–A Mathematical Programming Language [40], TOMLAB–a MATLAB environment for optimization [41], LINGO [42], ASCEND [43], LANCELOT [44], DASH [45] among others, which together with a gradient-based method, can be applied to solve the optimization problems proposed in the this paper.

4. Results and discussion

4.1. Minimization of $E_{L,tot}$ for a fixed cooling capacity

The model was used to determine simultaneously the optimal operation conditions and the optimal sizes of the process units that minimize the total exergy loss of the system $E_{L,tot}$ (objective function) while satisfying a refrigerating requirement of 50.0 kW. Formally, the proposed optimization problem, hereafter named as OP1, can be mathematically expressed as follows:

Problem OP1.

$$\begin{aligned} &\textit{Minimize } E_{L,tot} \\ &\text{s.t.} \\ &\begin{cases} \mathbf{h}_s(\mathbf{x}) = 0, \ \forall s \\ \mathbf{g}_t(\mathbf{x}) \leqslant 0, \ \forall t \\ Q_{EVAP} = 50 \text{ kW} \end{cases} \end{aligned} \tag{28}$$

where $\mathbf{x}$ is the vector of model variables, $\mathbf{h}_s(\mathbf{x})$ refers to equality constraints (mass, energy and exergy balances, correlations for physicochemical properties estimation, and design specifications), and $\mathbf{g}_t(\mathbf{x})$ refers to inequality constraints, which are used, for instance, to avoid temperature cross situations and to impose lower and upper bounds on some critical operating variables.

As a result, the proposed optimization problem OP1 provides:

- Minimal $E_{L,tot}$ and its distribution among the process units.
- Optimal values of temperature, pressure, composition and flow rate of all process streams,
- Optimal values of heat transfer area (HTA) of all process units.

For a required cooling capacity of 50.0 kW, the computed minimal $E_{L,tot}$ value is 5.159 kW (asymptotic value) demanding a THTA of 158.462 m^2, i.e. $E_{L,tot}$ can no longer be improved with a THTA larger than 158.462 m^2. Moreover, as is discussed later in Problem OP4, it was observed that a $E_{L,tot}$ value of 5.160 kW requires a THTA of 100.0 m^2. Since this insignificantly variation of less than 0.02% in $E_{L,tot}$ with respect to the optimal solution (5.159 kW) leads to a very significant reduction of 36.89% in THTA, a minimal $E_{L,tot}$ value of 5.160 kW with a THTA value of 100.0 m^2 is considered a very good suboptimal solution for OP1 for the purpose of this work.

The optimal values of mass flow rate (M), temperature (T), pressure (P), and composition (X) of each process stream corresponding to the suboptimal solution are listed in Table 3; the optimal values of individual exergy loss (E_L), heat transfer area (HTA), logarithmic mean temperature difference ($LMTD$), and heat load (Q) in each process unit are listed in Table 4.

It can be observed in Table 4 that the absorber is the process unit that contributes most to $E_{L,tot}$ (around 41.70%) followed by the condenser (19.82%) and the evaporator (15.93%). The optimal exergy loss rate in the generator and the solution heat exchanger are lower than the other process units and they contribute almost equally to the minimal $E_{L,tot}$ (11.31 and 11.22%, respectively).

On the other hand, the evaporator requires 60.308 m^2 and it is the process unit with the highest HTA, followed by the absorber, condenser, and generator, which require HTA values of 20.725, 11.221, and 7.342 m^2, respectively. The solution heat exchanger only requires 0.403 m^2, and it is the process unit with the lowest requirement of HTA. It is worth mentioning that, as in this particular case the THTA value is 100.0 m^2, the reported individual HTA values represent directly the percentage of distributed THTA among the process units.

The crystallization of the LiBr solution is a critical issue that must be considered to ensure a feasible and proper operating mode. Therefore, it is interesting to see how far (or close) the operating conditions are from the operating region with crystallization risk. Fig. 2 shows the Dühring chart for aqueous LiBr solutions [46], where diagonal lines represent constant LiBr concentration (mass fraction). It plots the optimal pressure, temperature and composition values of the streams of the refrigeration cycle obtained by minimization of $E_{L,tot}$ (in green solid lines). The other plotted refrigeration cycle (in magenta solid lines) corresponds to the model's optimal solution obtained by minimization of THTA, which is discussed in the next section. It should be noted that the computed solution was obtained without considering any constraint on the model decision variables, except for an upper bound on the LiBr concentration for preventing that the LiBr crystallization curve is exceeded and inequality constraints for preventing temperature and pressure crosses in process units.

As shown in Fig. 2, although the thermodynamic conditions of the stream leaving the expansion valve EV2 and entering the absorber (stream 6, X_6 = 63.551%, P_6 = 1.442 kPa, and T_6 = 63.91 °C) are not coinciding with a point of the crystallization line, the margin of safety is critical because the computed optimal operating point is near by the crystallization curve.

Table 3
Operation condition values by minimizing the total system exergy loss rate ($E_{L,tot}$).

Point	M (kg s^{-1})	T (°C)	P (kPa)	X (%)
1	0.18696	45.5	1.442	56.294
2	0.18696	45.5	7.080	56.294
3	0.18696	68.1	7.080	56.294
4	0.16578	91.5	7.080	63.513
5	0.16578	63.9	7.080	63.513
6	0.16578	63.9	1.442	63.513
7	0.02118	91.5	7.080	0.00
8	0.02118	39.1	7.080	0.00
9	0.02118	12.3	1.442	0.00
10	0.02118	12.3	1.442	0.00
11	1.000	27.0	101.0	0.00
12	1.000	39.6	101.0	0.00
13	109.469	13.0	101.0	0.00
14	109.469	12.9	101.0	0.00
15	0.453	30.0	101.0	0.00
16	0.453	63.4	101.0	0.00
17	0.029	92.0	75.41	0.00
18	0.029	92.0	75.41	0.00

Table 4
Heat transfer area, LMTD, heat load, and exergy loss rate values of process units by minimizing the total system exergy loss rate ($E_{L,tot}$).

	E_L (kW)	HTA (m^2)	LMTD (°C)	Q (kW)
ABS	2.152	20.725	4.374	63.461
GEN	0.584	7.342	6.046	66.586
EVAP	0.822	60.308	0.553	50.00 [a]
COND	1.023	0.139[b]/11.082[c] 11.221[d]	6.426[b]/1.837[c]	2.239[b]/50.887[c] 53.125 [d]
SHE	0.579	0.403	20.782	8.381
Total	5.160	100.0		

[a] Fixed value.
[b] Sensible heat (COND1).
[c] Condensation heat (COND2).
[d] Total.

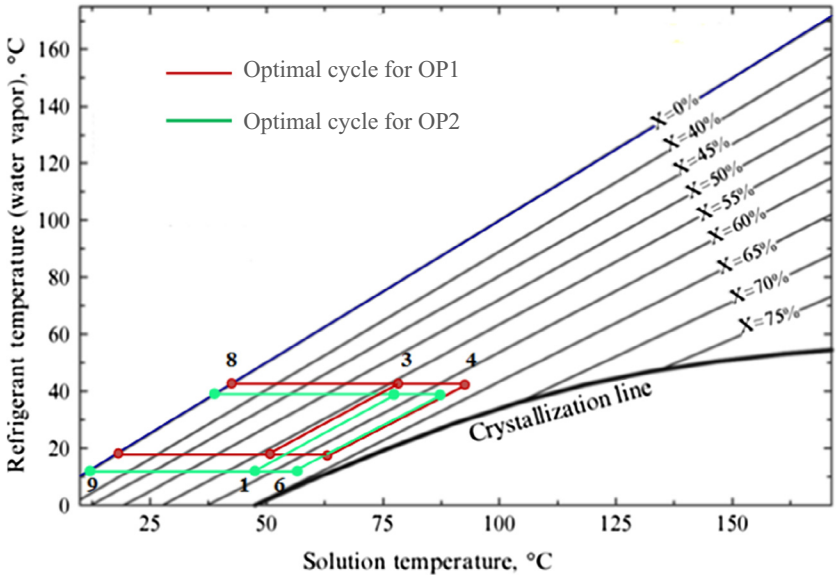

Fig. 2. Dühring chart for aqueous LiBr solutions taken from [46]. Representation of the optimal solutions resulting from the optimization problems OP1 and OP2.

The optimal solution for OP1 can be effectively used not only as good initial guess values for the local nonlinear optimization solver when the total cost (investment and operating costs) is proposed as objective function to be minimized, but also in a global optimization algorithm independently of the proposed objective function; certainly, good variable bounds are essential in global optimization approaches in order to achieve convergence at low computational cost (few iterations and short CPU times).

4.2. Minimization of THTA for a fixed cooling capacity

The mathematical model is here used to solve a second optimization problem consisting on the minimization of total heat transfer area THTA (objective function) for the same cooling capacity assumed in the previous section (50.0 kW). Formally, the proposed optimization problem, hereafter named as OP2, can be mathematically expressed as follows:

Problem OP2.

$$\begin{aligned} &\textit{Minimize } \text{THTA} \\ &\text{s.t.} \\ &\begin{cases} \mathbf{h}_s(\mathbf{x}) = 0, \ \forall s \\ \mathbf{g}_t(\mathbf{x}) \leqslant 0, \ \forall t \\ Q_{EVAP} = 50 \text{ kW} \end{cases} \end{aligned} \tag{29}$$

where $\mathbf{x}$ (the vector of model variables), $\mathbf{h}_s(\mathbf{x})$ (mass, energy and exergy balances, correlations for physicochemical properties estimation, and design specification), and $\mathbf{g}_t(\mathbf{x})$ (inequality constraints) are similar as considered in the previous problem OP1. The only difference between OP1 and OP2 is the considered objective function.

As a result, the proposed optimization problem OP2 provides:

- Minimal THTA and its distribution among the process units.
- Optimal values of temperature, pressure, composition and flow rate of all process streams,
- Optimal values of E_L in each process unit.

The obtained optimal results are listed in Table 5 and 6. They show that the minimal THTA required is 16.0 m^2, which determines a $E_{L,tot}$ value of 9.429 kW (Table 6). This means that a THTA smaller than 16.0 m^2 cannot comply with the specified cooling capacity of 50.0 kW. In other words, fixing a THTA value smaller than 16.0 m^2 will result in an infeasible solution of the optimization problem since the OP2 constraint specifying a required cooling capacity of 50.0 kW cannot be satisfied.

The THTA value decreases 84.00% with respect to the value obtained when minimizing $E_{L,tot}$ (from 100.0 to 16.0 m^2) while $E_{L,tot}$

Table 5
Operation condition values by minimizing the total system heat transfer area (THTA).

Point	M (kg s^{-1})	T (°C)	P (kPa)	X (%)
1	0.25706	38.9	0.823	57.985
2	0.25706	38.9	5.723	57.985
3	0.25706	63.6	5.723	57.985
4	0.23590	86.0	5.723	63.187
5	0.23590	57.8	5.723	63.187
6	0.23590	57.8	0.823	63.187
7	0.02116	86.0	5.723	0.000
8	0.02116	35.2	5.723	0.000
9	0.02116	4.2	0.823	0.000
10	0.02116	4.2	0.823	0.000
11	25.403	27.0	101.0	0.000
12	25.403	27.5	101.0	0.000
13	119.332	13.0	101.0	0.000
14	119.332	12.9	101.0	0.000
15	31.763	30.0	101.0	0.000
16	31.763	30.5	101.0	0.000
17	0.031	92.0	75.41	0.000
18	0.031	92.0	75.41	0.000

Table 6
Heat transfer area, LMTD, heat load, and exergy loss rate values of process units by minimizing the total system heat transfer area (THTA).

	E_L (kW)	HTA (m^2)	LMTD (°C)	Q (kW)
ABS	3.726	5.769	16.477	66.543
GEN	1.124	3.247	14.322	69.763
EVAP	2.455	3.803	8.764	50.000[a]
COND	1.271	0.035[b]/2.550[c] 2.585[d]	25.148[b]/8.001[c]	2.205[b]/51.015[c] 53.220[d]
SHE	0.853	0.594	20.602	12.245
Total	9.429	16.0		

[a] Fixed value.
[b] Sensible heat (COND1).
[c] Condensation heat (COND2).
[d] Total.

Table 7
Parameter values for estimating process unit investment Z_k (Eq. (26)).

Unit k	A_k	B_k	C_k
GEN	1800	0.8	24,915
EVAP	5900	0.552	0
ABS	9.976	1.820	0
COND	2119	0.497	0
SHE	2674	0.465	0

increases 82.73% (from 5.160 to 9.429 kW). Then, it is found that 9.429 kW represents an upper bound for the total exergy loss rate when the total heat transfer area is minimized using a LiBr-H_2O single-effect ARS for a required cooling capacity of 50.0 kW, and for the considered system specifications and model assumptions.

It can also be observed that the absorber is the process unit that contributes most to THTA with 36.05%. The evaporator and generator contribute almost similarly to THTA, with 23.76 and 20.31%, respectively, while the condenser contributes with 16.15%. The solution heat exchanger contributes to THTA with only 3.71%.

As expected, the reduction in THTA is accompanied by a generalized increase of the temperature and mass flow rate values of all process streams in the high thermal-level region. Indeed, higher LMTD values are computed for OP2 than OP1.

By comparing the results reported in Table 4 ($E_{L,tot}$ minimization) with those in Table 6 (THTA minimization), it can be clearly observed that the order of the relative importance of the process units contribution to the total exergy loss rate is the same in OP1 and OP2, but this order changes for THTA; that is, the evaporator has the largest HTA followed by the absorber in OP1, but this relative order is altered in OP2.

Finally, it can be observed in the Duhring chart (Fig. 2) that the thermodynamic conditions computed for stream 6 in OP2 (X_6 = 63.187%, P_6 = 0.823 kPa, and T_6 = 57.8 °C) lead to an operating point closer to the crystallization limit than OP1, resulting in a higher crystallization risk.

4.3. Minimization of the total annual cost (TAC) for a fixed cooling capacity

The optimization problems OP1 and OP2 determined, respectively, a (sub)minimal $E_{L,tot}$ of 5.160 kW with a "theoretical" THTA of 100.0 m^2 (OP1), and a minimal THTA of 16.0 m^2 with a maximal $E_{L,tot}$ of 9.429 kW (OP2), for a cooling capacity of 50.0 kW. It is then interesting to obtain the minimal total annual cost–computed by Eq. (23)–within the range from the minimal to the maximal values of THTA, and to see how the operating expenditures (OPEX) and capital expenditures of process units (CAPEX) contribute to the optimal TAC, as well as the values of the main decision variables at the economic optimum. Thus, a third optimization problem OP3 is proposed, which is formally expressed as follows:

Problem OP3.

$$\begin{aligned} &\textit{Minimize } \text{TAC} \\ &\text{s.t.} \\ &\begin{cases} \mathbf{h}_s(\mathbf{x}) = 0, \quad \forall s \\ \mathbf{g}_t(\mathbf{x}) \leqslant 0, \quad \forall t \\ Q_{EVAP} = 50 \text{ kW} \\ 16 \text{ m}^2 \leqslant THTA \leqslant 100 \text{ m}^2 \end{cases} \end{aligned} \tag{30}$$

In OP3, the constraints of the cost model are added to the equality $\mathbf{h}_s(\mathbf{x})$ and inequality $\mathbf{g}_t(\mathbf{x})$ constraints considered in OP1 and OP2. In OP3, THTA is an optimization variable that is allowed to vary between a lower bound of 16.0 m^2 (from OP2) and an upper bound of 100 m^2 (from OP1). The proposed optimization problem OP3 provides:

- Minimal TAC and its optimal distribution between CAPEX and OPEX.
- Optimal sizes of the process units.
- Optimal values of temperature, pressure, composition, and flow rate of all process streams.

The main results are presented in Figs. 3 and 4 and Tables 8 and 9. Fig. 3 shows the contribution of CAPEX and OPEX to TAC, and of the cost items to CAPEX and OPEX. Fig. 4 shows the contribution of each process unit to the total heat transfer area and to the total exergy loss rate. Tables 8 and 9 compare the stream temperature and heat transfer area values, respectively, obtained for the three objective functions (min. THTA, min. $E_{L,tot}$, and min. TAC).

As shown in Fig. 3a, the computed minimal TAC is 21422.5$/yr, of which 76.1% corresponds to CAPEX (16308.6$/yr) and 23.9% to OPEX (5113.9$/yr). The results shown in Fig. 3b indicate that the generator and evaporator are the process units that contribute most to CAPEX, which together represent approximately 70% of CAPEX (38.69% for GEN and 31.97% for EVAP). The absorber and condenser are the third and fourth largest contributors to CAPEX, which together represent around 25% of CAPEX (14.79% for ABS and 10.27% for COND). The solution heat exchanger presents the lowest contribution to CAPEX, with around 4.28%. The distribution of OPEX is shown in Fig. 3c.

On the other hand, Fig. 4 shows that the absorber is the largest contributor to both the total heat transfer area (33.19%, Fig. 4a) and the total exergy loss rate (39.16%, Fig. 4b). The condenser is the second largest contributor to THTA (25.46%, Fig. 4a) but the smallest contributor to $E_{L,tot}$ (9.73%, Fig. 4b). The generator is the third largest contributor to both THTA and $E_{L,tot}$, and the evaporator is the fourth to THTA and the second to $E_{L,tot}$, with 20.37% and 28.54%, respectively. The solution heat exchanger contributes with the smallest percentage to THTA (3.09%, Fig. 4a), and its contribution to $E_{L,tot}$ is similar as the condenser (around 10.0%).

Tables 8 and 9 compare the optimal values of some model variables obtained by minimizing $E_{L,tot}$ (OP1), minimizing THTA (OP2), and finally minimizing TAC (OP3) by setting the bounds on THTA obtained from OP1 and OP2. It can be observed in Table 8 that the optimal stream temperature values obtained from OP3 lie between the optimal values obtained from OP1 and OP2. Similarly, Table 9 shows that the heat transfer area (HTA) of the main system components (absorber, generator, evaporator, and condenser) computed by OP3 also lie between the optimal values computed by OP1 and OP2. Then, the optimal solutions computed for OP1 and OP2 systematically provide proper bounds for the main operating variables as well as for the sizes of the system components, which is of relevance to set good bounds when global optimization algorithms are used or to facilitate the model convergence when the cost optimization problem is solved for more complex process configurations.

The optimal concentration values of the weak and strong LiBr solutions obtained from OP3 were 58.7 and 63.4%, respectively, while the low (evaporator) and high (generator) pressure values were 0.837 and 5.730 kPa, respectively. The used lower and upper bounds for concentrations and pressures correspond to the lowest and highest values obtained from OP1 and OP2. The lower and upper bounds used for LiBr concentrations were 56.3 and 63.5%, respectively, which are the lowest and highest values obtained from OP1 (Table 3). On the other hand, the lower bound for pressure was 0.823 kPa, which was obtained from OP2 (Table 5), and the upper bound was 7.080 kPa, which was obtained from OP1 (Table 3).

4.4. Minimization of $E_{L,tot}$ for a wide range of available THTA values for a fixed cooling capacity

The aim of this section is to obtain the optimal solutions within the range from the minimal to the maximal values of THTA com-

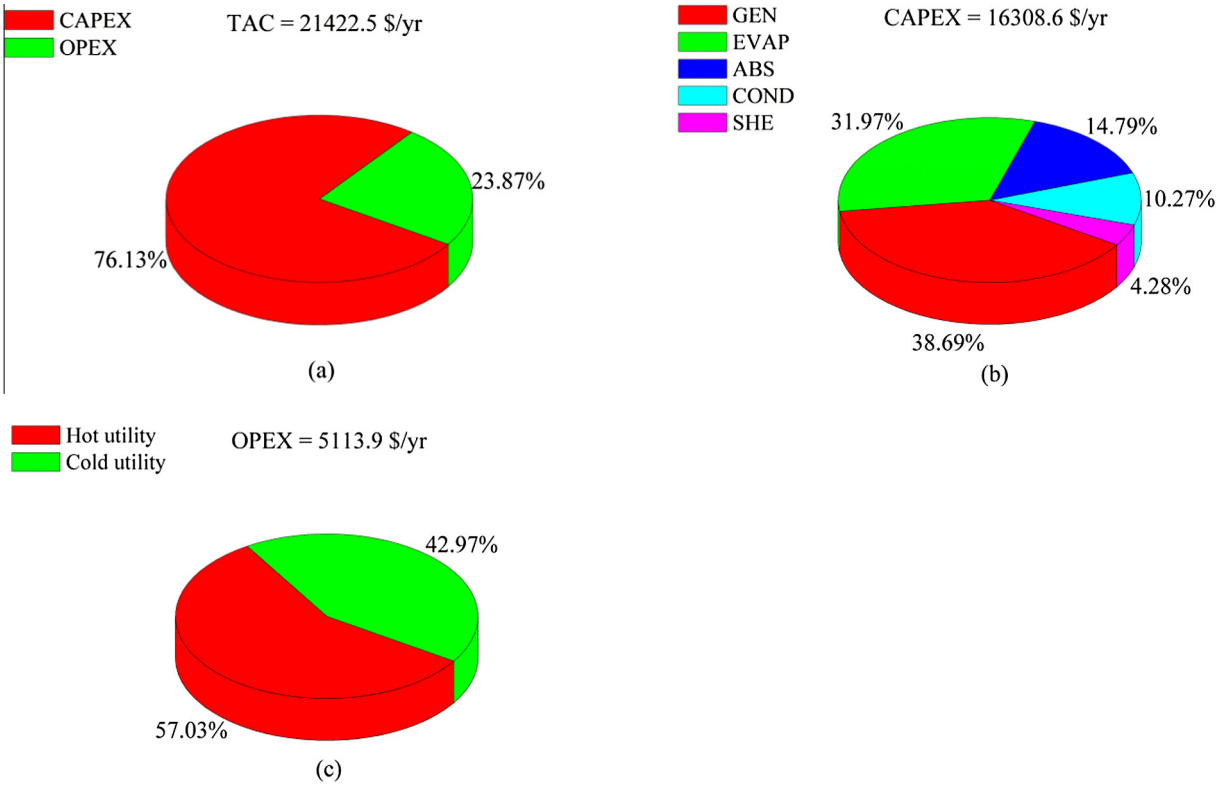

Fig. 3. Optimal total annual cost distribution. (a) Contribution of CAPEX and OPEX to TAC; (b) contribution of process units to CAPEX; (c) contribution of heating and cooling utilities to OPEX.

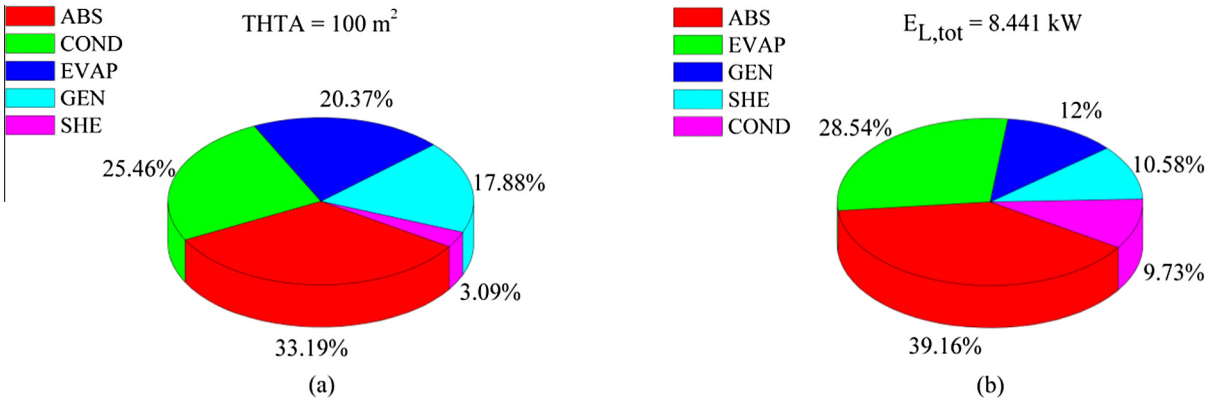

Fig. 4. Contribution of process units to (a) total heat transfer area (THTA) and (b) total exergy loss rate ($E_{L,tot}$).

puted from OP2 and OP1, respectively, and to investigate how the optimal operating conditions, process unit sizes and their relative sizes vary as THTA increases. For this, a fourth optimization problem OP4 is proposed, which is formally expressed as follows:

Problem OP4.

$$\begin{aligned} &\textit{Minimize } E_{L,tot} \\ &\text{s.t.} \\ &\begin{cases} \mathbf{h}_s(\mathbf{x}) = 0, \ \forall s \\ \mathbf{g}_t(\mathbf{x}) \leqslant 0, \ \forall t \\ Q_{EVAP} = 50 \text{ kW} \\ \text{THTA} = p_{THTA} \end{cases} \end{aligned} \tag{31}$$

The equality and inequality constraints in OP4 ($\mathbf{h}_s(\mathbf{x})$ and $\mathbf{g}_t(\mathbf{x})$, respectively) are the same as those in OP1 and OP2. In contrast to OP1 and OP2, a model parameter p_{THTA} referring to the THTA is defined and it is varied from 16.0 obtained in OP2 to 100.0 m^2 obtained in OP1.

As a result, the proposed optimization problem OP4 provides:

- Minimal $E_{L,tot}$ and its optimal distribution among the process units.
- Optimal distribution of the available THTA among the process units.
- Optimal values of temperature, pressure, composition, and flow rate of all process streams.

Table 8
Optimal temperature values of process streams from OP1, OP2, and OP3.

Point	Temperature (°C)		
	OP2 Min. THTA	OP3 Min. TAC	OP1 Min. $E_{L,tot}$
1	38.9	40.6	45.5
2	38.9	40.6	45.5
3	63.6	63.6	68.1
4	86.0	86.5	91.5
5	57.8	60.6	63.9
6	57.8	60.6	63.9
7	86.0	86.5	91.5
8	35.2	35.3	39.1
9	4.2	4.4	12.3
10	4.2	4.4	12.3
11	27.0[a]	27.0[a]	27.0[a]
12	27.5	33.8	39.6
13	13.0[a]	13.0[a]	13.0[a]
14	12.9	12.9	12.9
15	30.0[a]	30.0[a]	30.0[a]
16	30.5	39.3	63.4
17	92.0[a]	92.0[a]	92.0[a]
18	92.0[a]	92.0[a]	92.0[a]

[a] Fixed value (model parameter).

Table 9
Optimal values of heat transfer area of process units from OP1, OP2, and OP3.

Unit	HTA (m^2)		
	OP2 Min. THTA	OP3 Min. TAC	OP1 Min. $E_{L,tot}$
ABS	5.769	6.363	20.725
GEN	3.247	3.428	7.342
EVAP	3.803	3.906	60.308
COND	0.035[a]	0.059[a]	0.139[a]
	2.550[b]	4.822[b]	11.082[b]
SHE	0.594	0.593	0.403
Total	16.0	19.171	100.0

[a] Sensible heat (COND1).
[b] Condensation heat (COND2).

Figs. 5–18 present the resulting optimal values of the model variables for each fixed value of p_{THTA}; each plotted point belongs to an optimal solution. Thus, a complete optimal solution for a given value of p_{THTA} can be directly gathered from these figures.

For the total variation range of THTA, Fig. 5 indicates that the minimal $E_{L,tot}$ decreases 45.27%, from 9.429 kW for 16.0 m^2 to 5.160 kW for 100.0 m^2. Such a decrease is due to the individual contribution of each process unit (Fig. 5), which results from the optimal distribution values of THTA (Fig. 6), LMTD (Fig. 7) and heat loads (Fig. 8), which depend, in turn, on the stream temperature (Figs. 9–13) and pressure (Fig. 14), the mass flow rate of the strong and weak solutions and refrigerant (Fig. 15) and the mass flow rate of the utilities in each process unit (Figs. 16 and 17), and the concentration of the strong and weak solutions (Fig. 18); all varying simultaneously in each optimization run. It should be noted that the consideration of the mass flow rates of auxiliary services as optimization variables increases the degrees of freedom of the optimization problem, allowing a larger variation range of the stream temperatures to distribute optimally the heat transfer area in each process unit. Although the process units are hardly coupled in terms of mass and/or temperature, it is possible to identify the variables that have more influence on the performance of each unit.

Before presenting and discussing the results obtained for OP4, it is worth mentioning that (i) the individual exergy loss contribution

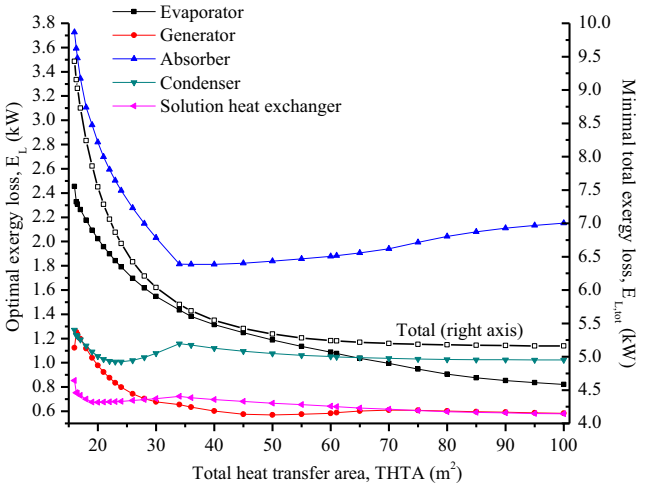

Fig. 5. Variation of the minimal total exergy loss rate of the whole system ($E_{L,tot}$) – right axis– and the optimal values of the exergy loss rate in each process unit (E_L) – left axis– with the available total heat transfer area (THTA).

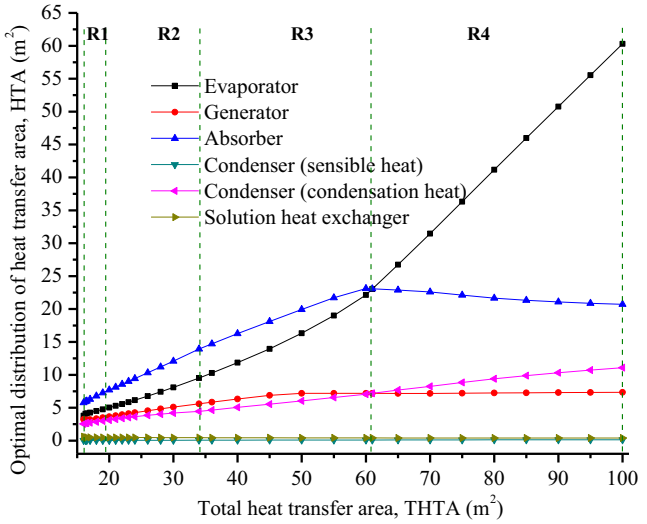

Fig. 6. Variation of the optimal values of the heat transfer area distributed to each process unit (HTA) with the available total heat transfer area (THTA), minimizing the total exergy loss rate ($E_{L,tot}$).

of each process unit to the total exergy loss rate and the heat transfer area distribution depend heavily on the available total heat transfer area THTA; (ii) at certain given THTA values, several process variables start modifying their tendencies significantly and other ones to a lesser extent, resulting in that the relative importance of the area distribution among certain units can change, or even invert, throughout the range of variation of THTA. That is why, for a better discussion of results, it is convenient to divide the total variation range of THTA into four subranges with these THTA values as the subrange extremes, and to analyze the behavior of the process units in each range separately. Based on this, the four subranges for THTA values are defined as follows: R1: from 16.0 to 19.0 m^2; R2: from 19.0 to 34.0 m^2; R3: from 34.0 to 61.0 m^2, and R4: from 61.0 to 100.0 m^2.

THTA range R1: from 16.0 to 19.0 m^2

Fig. 5 reveals that the minimal $E_{L,tot}$ significantly decreases from 9.429 to 7.859 kW when the available THTA increases from 16.0 to

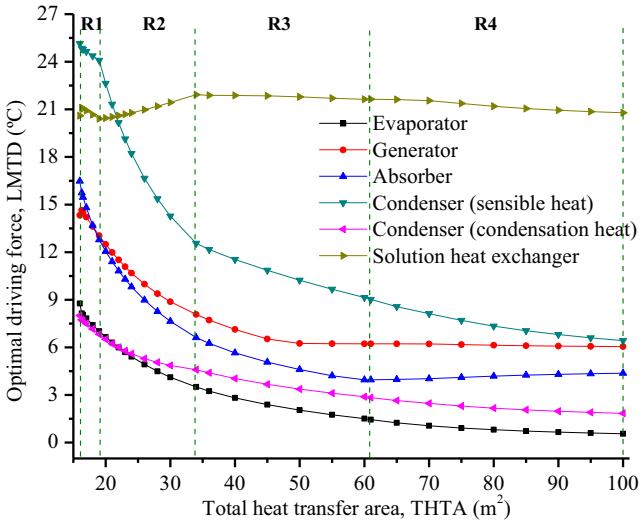

Fig. 7. Variation of the optimal values of the logarithm mean temperature difference (LMTD) in each process unit (driving force) with the available total heat transfer area (THTA), minimizing the total exergy loss rate ($E_{L,tot}$).

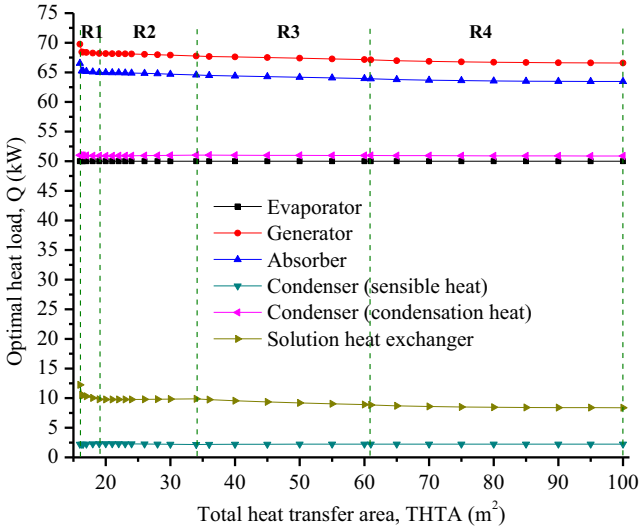

Fig. 8. Variation of the optimal values of the heat load in each process unit (Q) with the available total heat transfer area (THTA), minimizing the total exergy loss rate ($E_{L,tot}$).

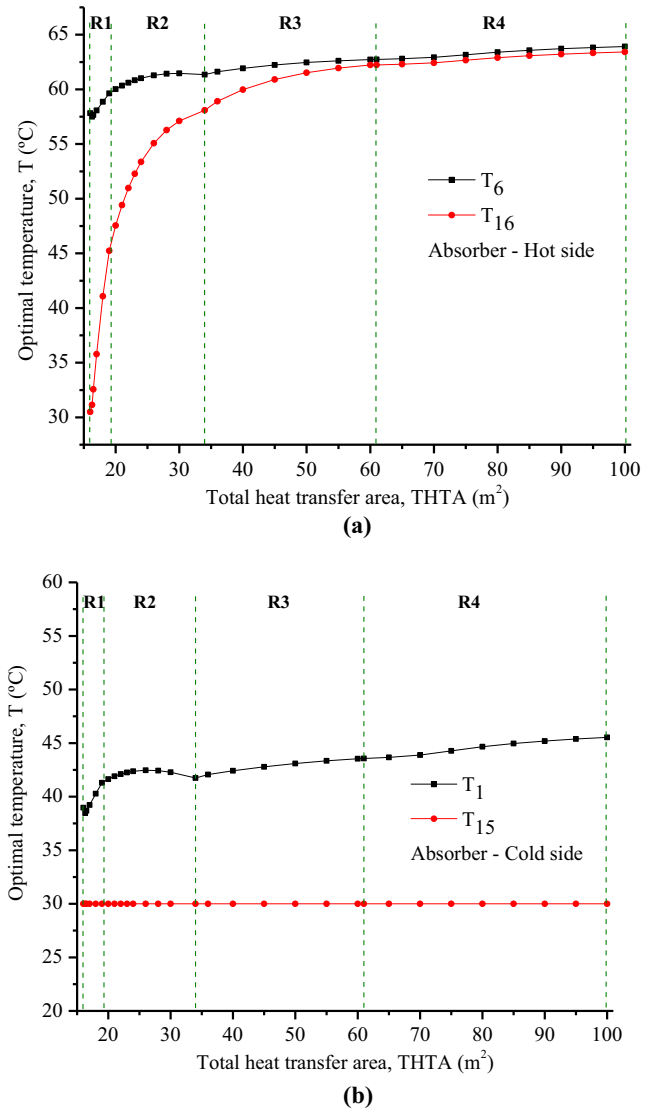

Fig. 9. Absorber (ABS). Variation of the optimal temperature values of the leaving cooling water (T_{16}) and the entering stream #6 (T_6) at the hot side (a); and the entering cooling water (T_{15}) and the leaving stream #1 (T_1) at the cold side (b), minimizing the total exergy loss rate ($E_{L,tot}$).

19.0 m^2 due to the decrease of the exergy loss rate in all process units. In this range, the major contributors to $E_{L,tot}$ are the absorber and evaporator followed by the condenser, generator, and solution heat exchanger. The $E_{L,ABS}$ value decreases from 3.726 kW (for 16.0 m^2) to 2.96 kW (for 19.00 m^2), and it is larger than the $E_{L,EVAP}$, which decreases from 2.455 kW (for 16.0 m_2) to 2.093 kW (for 19.0 m^2). The $E_{L,COND}$ and $E_{L,GEN}$ values are similar and they slightly decrease from 1.271 and 1.124 kW (for 16.0 m^2) to 1.091 and 1.041 kW (for 19.0 m^2), respectively. The solution heat exchanger is the process unit with the smallest exergy loss contribution, with $E_{L,SHE}$ values varying from 0.8532 to 0.6752 kW in this THTA range.

The individual E_L contribution of each process unit to $E_{L,tot}$ corresponds with the distribution of THTA in each unit. Fig. 6 shows that the absorber has the largest fraction of THTA, which is followed by the evaporator. The fractions of THTA distributed to the generator and the condenser (condensation heat) are practically the same. As available THTA increases, its distribution among them (ABS, EVAP, GEN, and COND for latent heat) follows a linear functionality. The amount of heat transfer area allocated to SHE and COND for sensible heat are the lower values, which are virtually identical and remain practically constant in this range (as well as throughout the other THTA ranges).

The optimal distribution of THTA among the process units shown in Fig. 6 corresponds to the optimal driving forces and heat loads depicted in Figs. 7 and 8, respectively.

From the optimization results, it can be clearly observed that the optimal THTA allocation is more influenced by the driving force than the heat loads. In fact, as the THTA increases, the optimal driving forces decrease (Fig. 7) and the corresponding optimal heat loads remain almost constant (Fig. 8) due to the variations of the optimal temperature values (Figs. 9–13) –with the related pressure values (Fig. 14)–, and the mass flow rates (Figs. 15–17).

Next, an analysis is presented to identify the key variables of each process unit that most affect the material and energy balances and the related driving forces that allow obtaining the optimal heat transfer area distribution indicated in Fig. 6.

For the absorber, the heat transfer area value HTA_{ABS} is computed from Eq. (32), where the logarithmic mean temperature difference value $LMTD_{ABS}$ is calculated by Eq. (33). Then, the energy balance for the absorber is given by Eqs. (34) and (35):

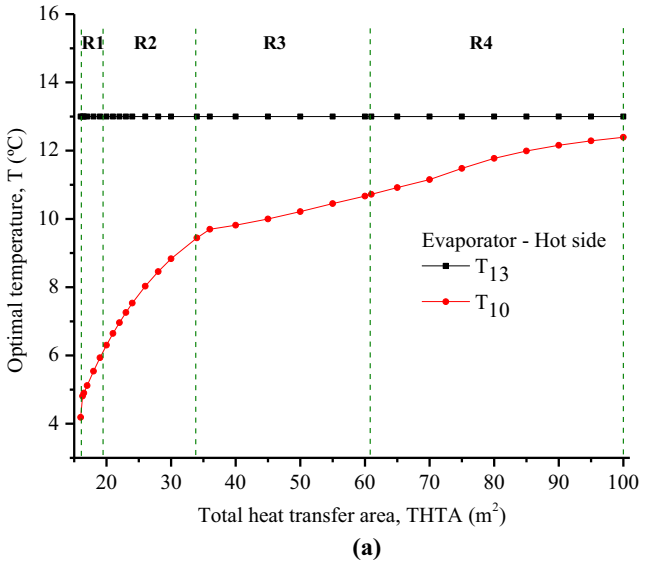

Fig. 10. Evaporator (EVAP). Variation of the optimal temperature values of the entering heating stream (T_{13}) and the leaving stream #10 (T_{10}) at the hot side (a); and the leaving heating stream (T_{14}) and the entering stream #9 (T_9) at the cold side (b), minimizing the total exergy loss rate ($E_{L,tot}$).

$$Q_{ABS} = U_{ABS} \cdot HTA_{ABS} \cdot LMTD_{ABS} \quad (32)$$

$$LMTD_{ABS} = \frac{(T_6 - T_{16}) - (T_1 - T_{15})}{\ln \frac{(T_6 - T_{16})}{(T_1 - T_{15})}} \quad (33)$$

$$Q_{ABS} = M_{15} \cdot \left(H_{15(T15)} - H_{16(T16)}\right) \quad (34)$$

$$Q_{ABS} = M_{10} \cdot H_{10(T10)} + M_6 \cdot H_{6(T6,X6)} - M_1 \cdot H_{1(T1,X1)} \quad (35)$$

According to Eq. (32), to increase HTA_{ABS} from 5.769 to 7.263 m^2 when THTA increases from 16.0 to 19.0 m^2 and Q_{ABS} is practically constant at 65.00 kW with a fixed U_{ABS} value of 0.70 (kW m^{-2} °C^{-1}), $LMTD_{ABS}$ should decrease from 16.47 to 12.78 °C. To achieve this reduction in $LMTD_{ABS}$, T_{16} increases significantly from 30.5 °C (value imposed by the inequality constraint: $T_{16} \geqslant T_{15} + 0.5$ °C) to 45.23 °C; in order to achieve this, it is necessary that the mass flow rate M_{15} decreases from 31.763 to 1.018 kg s^{-1} through the energy balance (Eq. (34)).

It is worth mentioning that, although the optimal temperature, mass flow rate and concentration values of the weak solution (T_1, M_1 and X_1, respectively) and strong solution (T_6, M_6 and X_6, respectively) and the optimal refrigerant flow rate (M_{10}) vary, their variations are not as pronounced as those observed for the optimal temperature and mass flow rate of the cooling water (T_{16} and M_{15}, respectively); for instance, T_1 increases only by 2.32 °C, from 38.97 to 41.29 °C, and X_1 and X_6 increase only around 1.5% (X_1 from 57.45 to 58.13% and X_6 from 63.19 to 64.36%). Even though these increases are small, they contribute to fulfill the energy balance given by Eqs. (34) and (35). Then, the mass and energy balances in the absorber are met with significant changes in some variables (T_{16} and M_{15} in this case) and small variations in other ones (T_1, M_1, X_1, M_6, X_6, T_6).

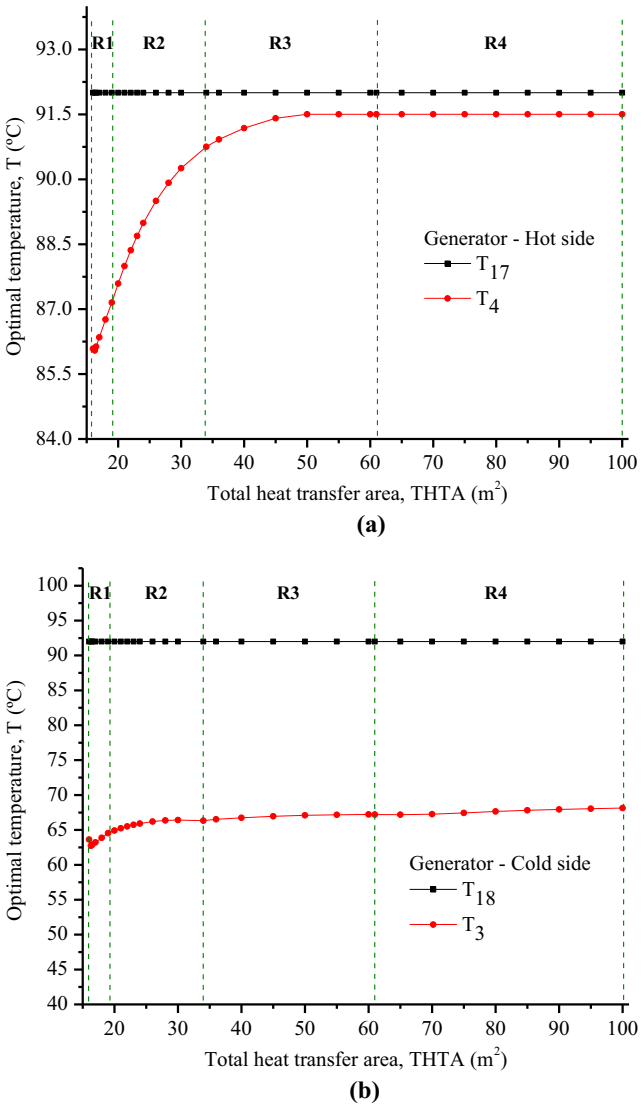

Fig. 11. Generator (GEN). Variation of the optimal temperature values of the entering cooling water (T_{17}) and the leaving stream #4 (T_4) at the hot side (a); and the leaving cooling water (T_{18}) and entering stream #3 (T_3) at the cold side (b), minimizing the total exergy loss rate ($E_{L,tot}$).

By a similar analysis for the evaporator, temperature T_9 results to be the most influential variable in the optimal allocation of THTA to it, which increases 1.75 °C, from 4.18 to 5.93 °C. This increase determines a lower latent heat of vaporization and, according to the liquid-vapor equilibrium of steam, this implies a small decrease of the optimal mass flow rate of refrigerant (M_{10}) to meet the corresponding energy balance in EVAP (from $2.116 \cdot 10^{-2}$ to $2.109 \cdot 10^{-2}$ kg s^{-1}).

Similarly, it is possible to identify that the decrease of the optimal values of both driving forces $LMTD_{COND1}$ and $LMTD_{COND2}$ in the

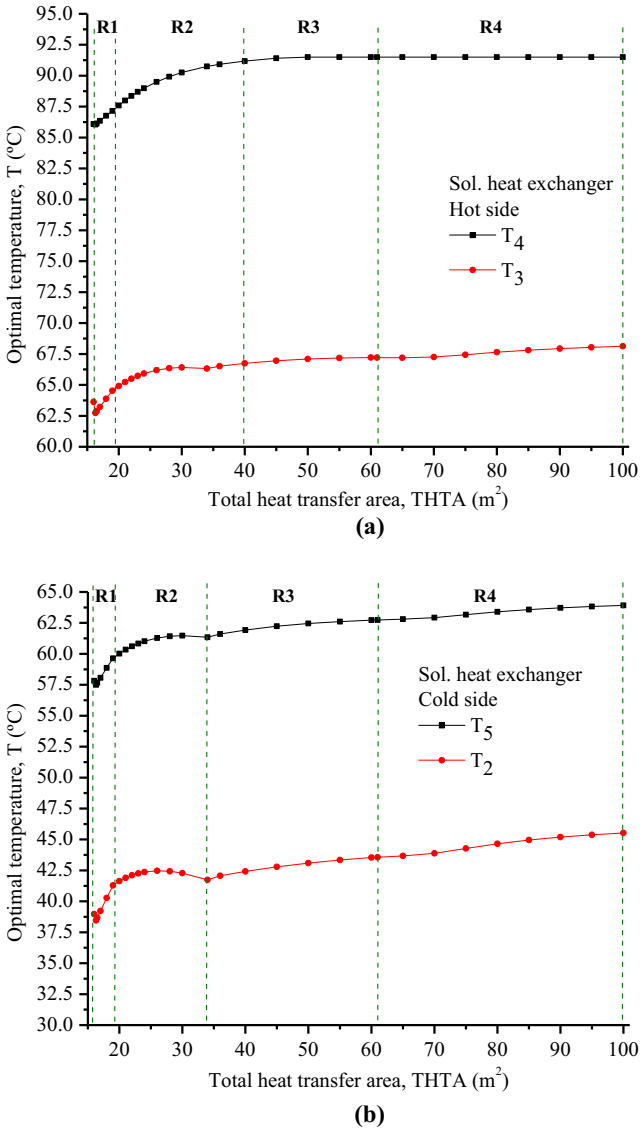

Fig. 12. Solution heat exchanger (SHE). Variation of the optimal temperature values of the leaving stream #3 (T_3) and the entering stream #4 (T_4) at the hot side (a); and the entering stream #2 (T_2) and leaving stream #5 (T_5) at the cold side (b), minimizing the total exergy loss rate ($E_{L,tot}$).

condenser is mainly due to the variation of T_7 and T_8 since T_{12} and T^* reach the limits imposed in the model ($T^* \geqslant T_{11} + 0.2$ and $T_{12} \geqslant T_{11} + 0.2$). For increasing values of THTA, Fig. 13a and b clearly show that T_8 decreases from 35.24 to 34.06 °C and T_7 increases from 86.08 to 87.15 °C, so that $LMTD_{COND1}$ and $LMTD_{COND2}$ decrease from 25.14 to 24.08 °C and from 8.00 to 6.82 °C, respectively. Figs. 15 and 16 show the optimal values of the mass flow rates at the condenser related to these variations (M_7 and M_{11}).

THTA range R2: from 19.0 to 34.0 m²

In this subrange of available THTA, the minimal $E_{L,tot}$ value decreases from 7.859 kW for 19.0 m² to 5.783 kW for 34.0 m² due mainly to the decrease of the optimal exergy loss rate values in the absorber and evaporator, from 2.960 to 1.813 kW and from 2.093 to 1.435 kW, respectively (Fig. 5). Although the optimal exergy loss rate values of the remaining process units (COND, GEN, and SHE) vary with THTA, their variations are much less pronounced than the ones for ABS and EVAP. Regarding the order of relevance of the exergy loss contributions of the process units, GEN and SHE invert their relative importance in this range as a consequence of the tendencies observed in range R1. That is, at the beginning of this range (THTA = 19.0 m²), the optimal value of $E_{L,GEN}$ is greater than $E_{L,SHE}$ (1.041 vs. 0.6752 kW), reaching the same value of 0.6962 kW when the available THTA is 28.0 m² because $E_{L,GEN}$ decreases and $E_{L,SHE}$ slightly increases. For an available THTA $\geqslant$ 28.0 m², the optimal exergy loss rate values in the generator are slightly lower than in the solution heat exchanger.

Fig. 6 shows that THTA is still distributed linearly in this range and that the order of its relative distribution among the process units is unchanged with respect to range R1. However, it can be seen that the values of HTA allocated to the absorber and evaporator are larger than the rest when compared to the range R1.

In the absorber, the optimal cooling water temperature T_{16} (Fig. 9a) and mass flow rate M_{15} (Fig. 17) continue increasing and decreasing, respectively, with increasing THTA, although these variations are less pronounced compared to R1. Indeed, T_{16} increases from 45.23 °C for 19.0 m² to 58.08 °C for 34.0 m² while M_{15} decreases from 1.018 to 0.549 kg s^{-1}, which leads to a $LMTD_{ABS}$ reduction from 12.78 to 6.62 °C and a HTA_{ABS} increase from 7.263 to 13.929 m². These variations imply small changes in T_1 and T_6, in the order of 1.0–1.5 °C, as shown in Fig. 9.

In the condenser, the optimal values of all temperatures (T_7, T_8, T_{11}, T^*, T_{12}) and mass flow rate (M_{11}) of the cooling water vary significantly compared to range R1 to reduce $LMTD_{COND1}$ (sensible heat) from 24.08 to 12.56 °C and $LMTD_{COND2}$ (vaporization latent heat) from 6.82 to 4.59 °C, and thereby, to increase the total area ($HTA_{COND1} + HTA_{COND2}$) from 3.02 to 4.517 m². In fact, Fig. 13b shows that T^*, instead of remaining constant at the imposed limit of 27.50 °C ($T^* \geqslant T_{11} + 0.50$ °C) as in range R1, increases from 27.50 to 39.06 °C, close to T_8. Meanwhile, T_8 and T_7 increase from 34.07 to 40.01 °C and from 87.15 to 90.75 °C, respectively. It is also observed that T_{12} increases from the limit value (27.50 °C imposed by $T_{12} \geqslant T_{11} + 0.5$) to 39.60 °C. Fig. 13b shows how the temperature difference ($T_8 - T^*$) at the cold side of the condenser decreases with increasing THTA. Furthermore, Fig. 16 shows that M_{11} significantly decreases exponentially from 25.39 to 1.01 kg s^{-1}. Importantly, the increase of T_8 (and therefore, the condenser pressure P_8) and the decrease of M_{11} imply that the optimal concentration values of the weak and strong solutions (X_1 and X_6, respectively) decrease accordingly to satisfy the mass and energy balances in both the absorber and the generator, according to the values shown in Fig. 18.

In the generator, temperature T_4 is the variable that varies most, which together with the variations of the optimal mass flow rate and composition values of the weak solution (M_1 and X_1) and strong solution (M_6 and X_6), and the mass flow rate of refrigerant (M_7), allows decreasing the $LMTD_{GEN}$ value from 13.043 to 8.08 °C, leading to increased values of optimally allocated heat transfer area to the generator, from 3.485 to 5.592 m².

THTA range R3: from 34.0 to 61.0 m²

In this range of THTA values, Fig. 5 shows that the minimal $E_{L,tot}$ decreases slightly from 5.783 kW for 34.0 m² to 5.236 kW for 61.0 m², tending to 5.160 kW, which is reached in the range R4. The fact that an increase of THTA does not result in a significant decrease of the minimal $E_{L,tot}$ is because the temperature approximations reach constant values approaching to zero, reducing thus the possibility of variation of these temperatures meaning that the limit for heat exchange is being approached at the hot side of the absorber (Fig. 9a), at the cold side of the evaporator (Fig. 10b), at the hot side of the generator (Fig. 11a), and at the hot side of the condenser for condensation heat (Fig. 13b).

Similar to range R2, Fig. 6 shows that the available THTA is mostly distributed in the absorber and the evaporator throughout

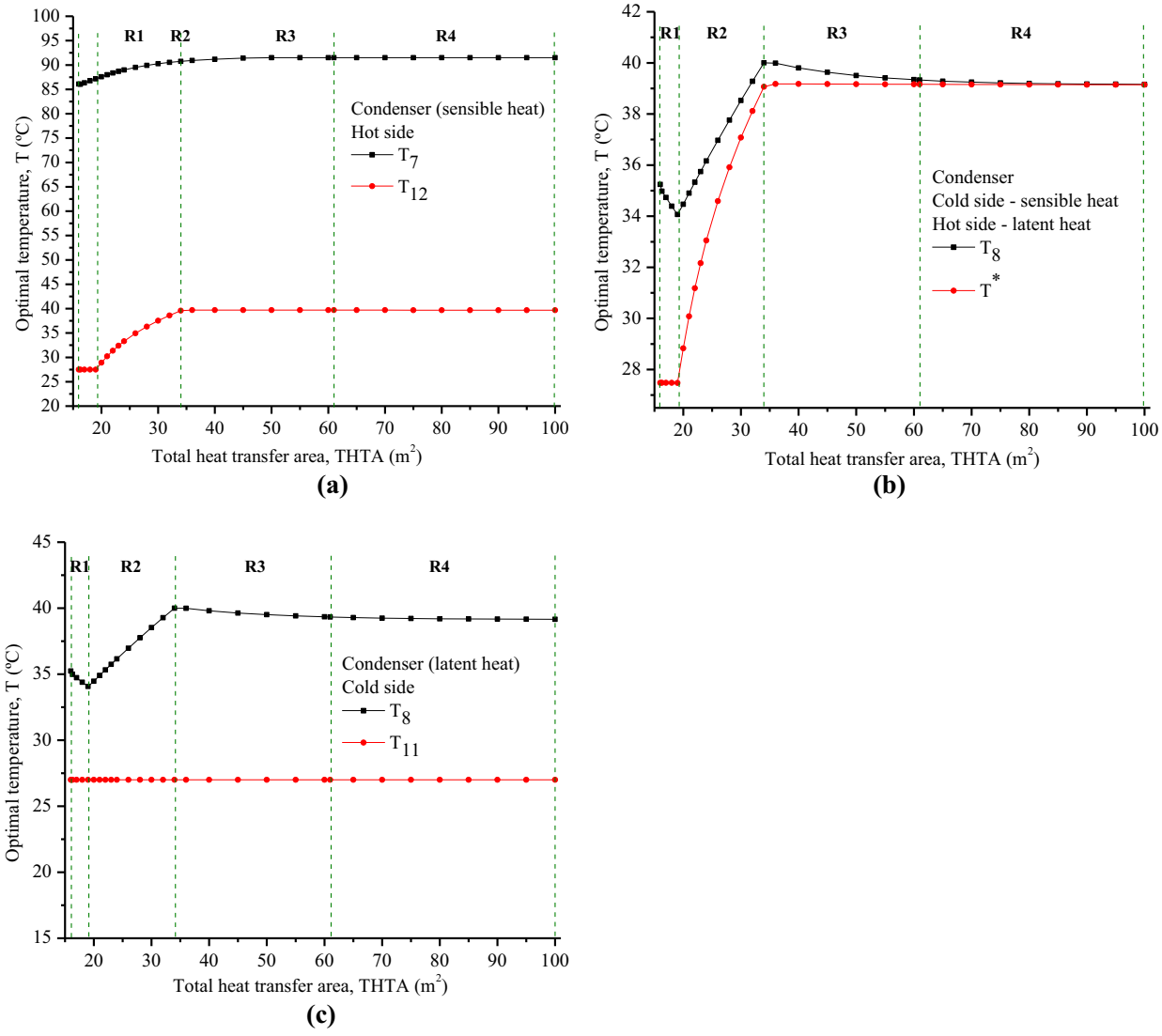

Fig. 13. Condenser (COND). Variation of the optimal temperature values of the leaving cooling water #12 (T_{12}) and the entering stream #7 (T_7) at the hot side (sensible heat) (a); the entering stream (T^*) and the leaving stream #8 (T_8) at the cold side (sensible heat) (b); and the entering cooling water (T_{11}) and the leaving stream #8 (T_8) at the cold side (condensation heat) (c), minimizing the total exergy loss rate ($E_{L,tot}$).

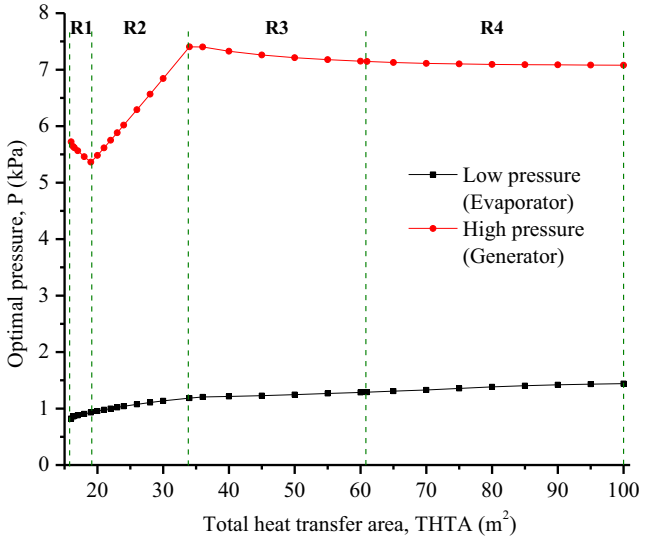

Fig. 14. Variation of the optimal values of the low and high operating pressure (P) – in evaporator and generator, respectively– with the available total heat transfer area (THTA), minimizing the total exergy loss rate ($E_{L,tot}$).

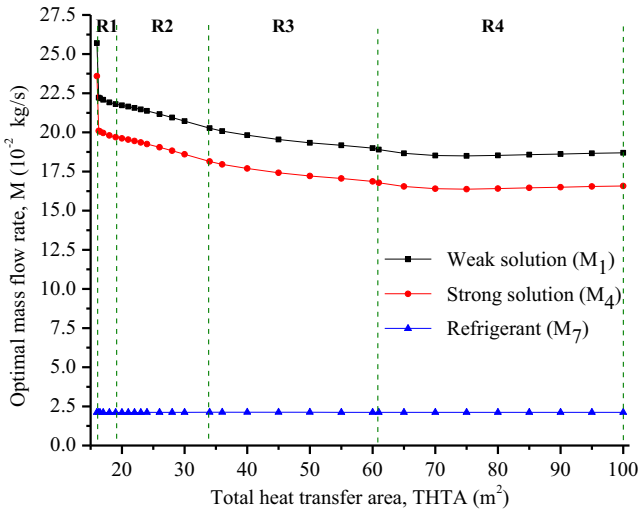

Fig. 15. Variation of the optimal mass flow rate values of the weak (M_1) and strong (M_6) LiBr solutions and refrigerant (M_7) with the available total heat transfer area (THTA), minimizing the total exergy loss rate ($E_{L,tot}$).

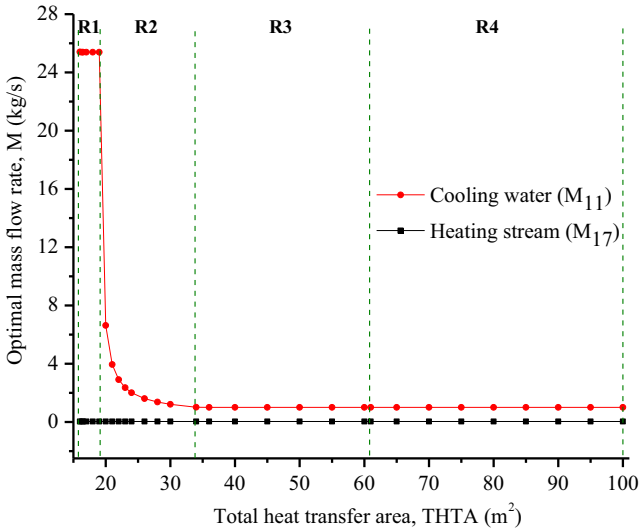

Fig. 16. Variation of the optimal mass flow rate values of the cooling water (M_{11}) and heating stream (M_{17}) with the available total heat transfer area (THTA), minimizing the total exergy loss rate ($E_{L,tot}$).

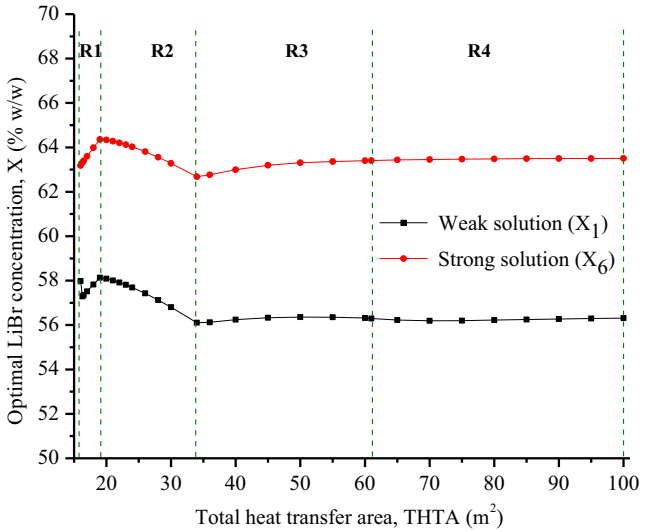

Fig. 18. Variation of the optimal concentration values of the weak (X_1) and strong (X_6) LiBr solutions with the available total heat transfer area (THTA), minimizing the total exergy loss rate ($E_{L,tot}$).

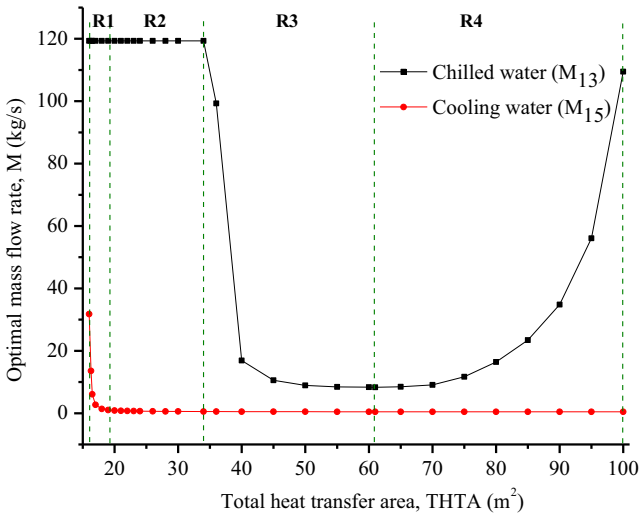

Fig. 17. Variation of the optimal mass flow rate values of the chilled water (M_{13}) and cooling water (M_{15}) with the available total heat transfer area (THTA), minimizing the total exergy loss rate ($E_{L,tot}$).

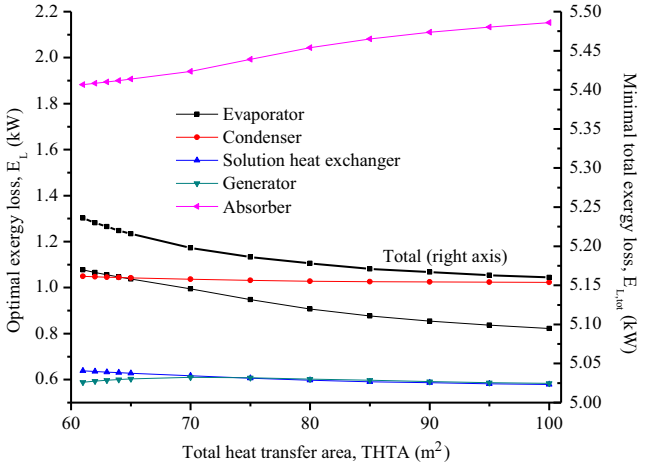

Fig. 19. Variation of the minimal total exergy loss rate of the whole system ($E_{L,tot}$) – right axis– and the optimal values of the exergy loss rate in each process unit (E_L) – left axis– with the available total heat transfer area (THTA) values corresponding to the range R4.

this range R3, but the optimal HTA allocated to the evaporator increases faster than the absorber with increasing THTA, contrarily to range R2. At the end of R3 (THTA = 61.0 m^2), it can be observed that HTA distributed in ABS and EVAP is the same (23.036 m^2). Variations of optimal HTA in GEN, COND, and SHE computed in this range are still small. A similar behavior between ABS and EVAP is also observed between GEN and COND. In this case, the optimal HTA allocated to COND increases faster than GEN with increasing THTA, reaching the same value (7.188 m^2) at the end of the range (THTA = 61.00 m^2).

THTA range 4: from 61.0 to 100.0 m^2

As shown in Fig. 5, with increasing available THTA, the minimal $E_{L,tot}$ decreases very smoothly from 5.236 kW for 61.0 m^2 to 5.160 kW for 100.0 m^2. To better visualize the results and elucidate the trade-offs among the variables in this range, the optimal exergy loss rate values of the process units are also plotted separately in Fig. 19. It can be observed that, while $E_{L,GEN}$, $E_{L,SHE}$, and $E_{L,COND}$ vary very slightly, $E_{L,EVAP}$ and $E_{L,ABS}$ vary more significantly and in an opposite way. Indeed, the optimal exergy loss rate values in GEN decreases from 0.589 to 0.584 kW (0.85%), in COND from 1.049 to 1.023 kW (2.48%), and in SHE from 0.638 to 0.579 kW (9.24%), while in EVAP the optimal exergy loss rate values decrease from 1.077 to 0.822 kW (23.67%) and in ABS they increase from 1.883 to 2.152 kW (14.28%). However, more importantly is to note that the optimal exergy loss rate values in EVAP and ABS decrease and increase, respectively, by almost the same (absolute) amount (0.255 and −0.269 kW, respectively) with practically no net effect on the minimal $E_{L,tot}$ values. Indeed, the resulting small difference between them is compensated by decreases of the exergy loss rate in the other process units without producing significant variations in the minimal $E_{L,tot}$ values with increasing available THTA to distribute.

The minimal $E_{L,tot}$ values depicted in Fig. 19 determine the optimal HTA distribution values shown in Fig. 6. It is observed that the decrease of the exergy loss rate in EVAP is due to a significant increase of its HTA, from 23.036 to 60.308 m^2 (161.30%), as a result

Table 10
Optimal temperature values of process streams from OP1 for theoretical and practical THTA values, OP2, and OP3.

Point	Temperature (°C)			
	OP2 Min. THTA	OP3 Min. TAC	OP1 Min. $E_{L,tot}$	
			100 m^2	61 m^2
1	38.9	40.6	45.5	43.6
2	38.9	40.6	45.5	43.6
3	63.6	63.6	68.1	67.2
4	86.0	86.5	91.5	91.5
5	57.8	60.6	63.9	62.7
6	57.8	60.6	63.9	62.7
7	86.0	86.5	91.5	91.5
8	35.2	35.3	39.1	39.3
9	4.2	4.4	12.3	10.7
10	4.2	4.4	12.3	10.7
11	27.0[a]	27.0[a]	27.0[a]	27.0[a]
12	27.5	33.8	39.6	39.1
13	13.0[a]	13.0[a]	13.0[a]	13.0[a]
14	12.9	12.9	12.9	11.5
15	30.0[a]	30.0[a]	30.0[a]	30.0[a]
16	30.5	39.3	63.4	62.2
17	92.0[a]	92.0[a]	92.0[a]	92.0[a]
18	92.0[a]	92.0[a]	92.0[a]	92.0[a]

[a] Fixed value (model parameter).

Table 11
Optimal values of heat transfer area of process units from OP1 for theoretical and practical THTA values, OP2, and OP3.

Unit	HTA (m^2)			
	OP2 Min. THTA	OP3 Min. TAC	OP1 Min. $E_{L,tot}$	
			100 m^2	61 m^2
ABS	5.769	6.363	20.725	23.077
GEN	3.247	3.428	7.342	7.188
EVAP	3.803	3.906	60.308	23.036
COND	0.035[a]	0.059[a]	0.139[a]	0.099[a]
	2.550[b]	4.822[b]	11.082[b]	7.190[b]
SHE	0.594	0.593	0.403	0.409
Total	16.0	19.171	100.0	61.00

[a] Sensible heat (COND1).
[b] Condensation heat (COND2).

of a reduction of the $LMTD_{EVAP}$ from 1.077 to 0.822 °C with variation of the outlet temperature of the refrigerant stream (T_{10}) and the outlet temperature of the chilled water (T_{14}) along with a significant increase of the mass flow rate of the latter (M_{13}) from 8.323 to 109.469 kg s^{-1}. In ABS, the increase of the exergy loss rate is due to a decrease of HTA from 23.077 to 20.725 m^2 requiring an increase of $LMTD_{ABS}$ from 1.883 to 2.152 °C with practically no variation of the mass flow rate of the cooling water (M_{15}).

Finally, Fig. 6 clearly shows that all increase of the available THTA implies virtually an increase of HTA in the evaporator, for which temperatures T_{10} and T_{14} and mass flow rate M_{13} conveniently vary, as shown in Fig. 10a, b, and 17, respectively. In fact, since the variations of HTA in both the generator and the solution heat exchanger are quite small and opposite (−2.14% and 1.46%, respectively) and the HTA in the absorber and the condenser decreases and increases, respectively, by almost the same amount with practically no net contribution to THTA, then the evaporator is the process unit whose variables have the greater variation range in order to distribute any additional increase of THTA, while modifying only slightly the variables of the other process units, but without improving the value of the objective function (minimization of $E_{L,tot}$), as discussed.

From the obtained results it can be concluded that 61 m^2 constitutes a "practical" upper bound for the total heat transfer area. This means that, if 61 m^2 is used as an upper bound for the minimization of the total exergy loss rate (OP1), the obtained optimal solution provides better upper bounds for the stream temperatures and the process unit sizes (except for the absorber) than the "theoretical" upper bound of 100 m^2, when the total annual cost is minimized (OP3), narrowing the variation range where the optimal values lie, as compared in Tables 10 and 11. This can result in a drastic reduction of the computational time if a global optimization algorithm is employed.

5. Conclusions

The application of the simultaneous optimization approach allowed to understand how all the trade-offs that exist among the process variables are elucidated when the total exergy loss rate, the total heat transfer area, and the total annual cost are minimized as single objective functions.

When the total exergy loss rate is minimized for a cooling capacity of 50 kW with no restrictions on the availability of the total heat transfer area and utilities (OP1), a value of 5.160 kW is computed for the total exergy loss rate, which implies a total heat transfer area of 100.0 m^2. The absorber is the process unit that contributes most to the total exergy loss (around 41.70%) while the evaporator is the unit with the largest contribution to the total heat transfer area (60.31%). When the total heat transfer area is minimized (OP2), a value of 16.0 m^2 is computed, which implies a total exergy loss rate of 9.429 kW. Compared to the previous optimization problem, the total heat transfer area is reduced by 84% and the total exergy loss rate is increased by 82.73%, which are accompanied by a general increase of temperatures as well as mass flow rates at the high thermal-level region (generator, solution heat exchanger, expansion valve, and absorber). The absorber is the process unit that contributes most to both the total heat transfer area (36.05%) and the total exergy loss (39.47%). The thermodynamic conditions of the stream leaving the expansion valve and entering the absorber computed for minimization of the total heat transfer area lead to an operating point closer to the crystallization limit, and thereby, to a higher risk for crystallization to occur than when the total exergy loss is minimized.

The optimal values of total heat transfer area computed by minimization of the total exergy loss rate (100 m^2) and the total heat transfer area (16 m^2) were used as an upper and a lower bound, respectively, to solve the minimization of the total capital and operating expenditures of the system (OP3). From an economical point of view, it was found that, for a cooling capacity of 50 kW, around three-quarters of the minimal total annual cost correspond to capital expenditures and the rest to operating expenditures, upon the model assumptions made and the given cost model. It was also found that the generator and evaporator represent together around 70% of the capital expenditures while the absorber is the largest contributor to both the total heat transfer area and the total exergy loss rate, with around 33.19 and 39.16%, respectively. From a methodological point of view, it was found that the optimal solutions computed for OP1 and OP2 provide proper bounds for stream temperatures as well as for the sizes of the system components. The relevance of this is that a systematic procedure can be developed to set good bounds when global optimization algorithms are used or to facilitate the model convergence when the cost optimization problem is solved for more complex process configurations.

In addition, the minimization of the total exergy loss rate for different values of available total heat transfer area comprised between the bounds computed in OP1 and OP2 was also per-

formed, allowing to see how the optimal distribution of the available total heat transfer area among the system components, as well as the operating conditions (stream temperature, pressure, composition, and mass flow rate) and heat loads, vary qualitatively and quantitatively with increasing available total heat transfer area. It was found that the order of relevance of the contribution of the system components to the total exergy loss rate depends on the available total heat transfer area value. For the lower total heat transfer area values, the absorber is the process unit with the largest reduction in the exergy loss rate and that contributes most to the reduction of the total exergy loss rate; in addition, it is the process unit with the largest heat transfer area. For the intermediate values of available total heat transfer area, the evaporator is the process unit with the largest reduction of the exergy loss and that contributes most to the reduction in the total exergy, thus inverting the tendency seen for the lower heat transfer area values; in addition, the evaporator shows the largest percentage increase in the total heat transfer area. For the higher values of available total heat transfer area, the added area is almost entirely allocated to the evaporator (95.57%) becoming definitively the largest system component, followed by the absorber; however, their absolute contributions to the total exergy loss rate are compensated by each other, leading to an asymptotic behavior of the total exergy loss rate with increasing total heat transfer area values. The optimization results indicated that no benefits can be obtained by increasing the available total heat transfer area above 61.0 m^2 since the minimal total exergy loss cannot be significantly improved by distributing more total area among the process units. Finally, it was also found that the optimal solution corresponding to 61 m^2 significantly improved the upper bound for the cost optimization problem with respect to 100 m^2, which can drastically reduce the computing time when global optimization algorithms are used.

As further work, the process units will be modeled with a higher level of detail; for instance, expressions to estimate the pressure drops and the overall heat transfer coefficients, and to consider design and geometrical characteristics of the process units, will be included in the model, as well as a more detailed cost model. The mathematical model will be extended to multi-effect systems.

Acknowledgement

The financial support from the Consejo Nacional de Investigaciones Científicas y Técnicas (CONICET) of Argentina and the Facultad Regional Rosario of the Universidad Tecnológica Nacional (UTN-FRRo) of Argentina is gratefully acknowledged.

References

[1] Morosuk T, Tsatsaronis G. A new approach to the exergy analysis of absorption refrigeration machines. Energy 2008;33:890–907. http://dx.doi.org/10.1016/j.energy.2007.09.012.
[2] Morosuk T, Tsatsaronis G. Advanced exergetic evaluation of refrigeration machines using different working fluids. Energy 2009;34:2248–58. http://dx.doi.org/10.1016/j.energy.2009.01.006.
[3] Cai D, He G, Tian Q, Tang W. Exergy analysis of a novel air-cooled non-adiabatic absorption refrigeration cycle with NH_3–NaSCN and NH_3–$LiNO_3$ refrigerant solutions. Energy Convers Manage 2014;88:66–78. http://dx.doi.org/10.1016/j.enconman.2014.08.025.
[4] Kaynakli O, Saka K, Kaynakli F. Energy and exergy analysis of a double effect absorption refrigeration system based on different heat sources. Energy Convers Manage 2015;106:21–30. http://dx.doi.org/10.1016/j.enconman.2015.09.010.
[5] El-Sayed YM, Gaggioli RA. A critical review of second law costing methods—I: background and algebraic procedures. J Energy Resour Technol 1989;111:1–7. http://dx.doi.org/10.1115/1.3231396.
[6] Gaggioli RA, El-Sayed YM. A critical review of second law costing methods—II: calculus procedures. J Energy Resour Technol 1989;111:8–15. http://dx.doi.org/10.1115/1.3231402.
[7] Misra RD, Sahoo PK, Gupta A. Thermoeconomic evaluation and optimization of a double effect H_2O/LiBr vapour-absorption refrigeration system. Int J Refrig 2005;28:331–43. http://dx.doi.org/10.1016/j.ijrefrig.2004.09.006.
[8] Farshi G, Mahmoudi SMS, Rosen MA, Yari M, Amidpour M. Exergoeconomic analysis of double effect absorption refrigeration systems. Energy Convers Manage 2013;65:13–25. http://dx.doi.org/10.1016/j.enconman.2012.07.019.
[9] Mosaffa AH, Garousi Farshi L, Infante Ferreira CA, Rosen MA. Exergoeconomic and environmental analyses of CO_2/NH_3 cascade refrigeration systems equipped with different types of flash tank intercoolers. Energy Convers Manage 2016;117:442–53. http://dx.doi.org/10.1016/j.enconman.2016.03.05.
[10] Gebreslassie BH, Groll EA, Garimella SV. Multi-objective optimization of sustainable single-effect water/lithium bromide absorption cycle. Renew Energy 2012;46(C):100–10.
[11] Morosuk T, Tsatsaronis G. Strengths and limitations of advanced exergetic analyses. In: ASME 2013 International mechanical engineering congress and exposition, 6B:1-11, Energy San Diego, California, USA, November 15–21. Conference Sponsors: ASME ISBN: 978-0-7918-5629-1.
[12] Chavez-Islas LM, Heard CL. Design and analysis of an ammonia-water absorption refrigeration cycle by means of an equation-oriented method. Ind Eng Chem Res 2009;48(4):1944–56. http://dx.doi.org/10.1021/ie800827z.
[13] Chavez-Islas LM, Heard CL. Optimization of a simple ammonia-water absorption refrigeration cycle by application of mixed-integer nonlinear programming. Ind Eng Chem Res 2009;48(4):1957–72. http://dx.doi.org/10.1021/ie800828w.
[14] Rubio-Maya C, Pacheco-Ibarra JJ, Belman-Flores JM, Galván-González SR, Mendoza-Covarrubias C. NLP model of a LiBr-H_2O absorption refrigeration system for the minimization of the annual operating cost. Appl Therm Eng 2012;37:10–8. http://dx.doi.org/10.1016/j.applthermaleng.2011.12.035.
[15] Mazzei MS, Mussati MC, Mussati SF. NLP model-based optimal design of LiBr–H_2O absorption refrigeration systems. Int J Refrig 2014;38:58–70. http://dx.doi.org/10.1016/j.ijrefrig.2013.10.012.
[16] Gebreslassie BH, Guillén-Gosálbez G, Jiménez L, Boer D. Design of environmentally conscious absorption cooling systems via multi-objective optimization and life cycle assessment. Appl Energy 2009;86(9):1712–22. http://dx.doi.org/10.1016/j.apenergy.2008.11.019.
[17] Goedkoop M, Spriensma R. The eco-indicator 99: a damage oriented method for life cycle assessment, methodology report. 2nd ed. Amersfoort (The Netherlands): PRé Consultants; 2000.
[18] Pieragostini C, Mussati M, Aguirre P. On process optimization considering LCA methodology. J Environ Manage 2012;96(1):43–54. http://dx.doi.org/10.1016/j.jenvman.2011.10.014.
[19] Brunet R, Reyes-Labarta JA, Guillén-Gosálbez G, Jiménez L, Boer D. Combined simulation–optimization methodology for the design of environmental conscious absorption systems. Comp Chem Eng 2012;46:205–16. http://dx.doi.org/10.1016/j.compchemeng.2012.06.030.
[20] Sayyaadi H, Nejatolahi M. Multi-objective optimization of a cooling tower assisted vapor compression refrigeration system. Int J Refrig 2011;34(1):243–56. http://dx.doi.org/10.1016/j.ijrefrig.2010.07.026.
[21] Jain V, Sachdeva G, Kachhwaha SS, Patel B. Thermo-economic and environmental analyses based multi-objective optimization of vapor compression–absorption cascaded refrigeration system using NSGA-II technique. Energy Convers Manage 2016;113:230–42. http://dx.doi.org/10.1016/j.enconman.2016.01.056.
[22] American Society of Heating R and A-CE. ASHRAE handbook: fundamentals. Atlanta (GA): ASHRAE; 1989.
[23] Rogers G, Mayhew Y. Engineering thermodynamics: work and heat transfer. 4th ed. Harlow (Essex, England) and New York: Longman Scientific; 1992.
[24] Kaita Y. Thermodynamic properties of lithium bromide–water solutions at high temperatures. Int J Refrig 2001;24:374–90. http://dx.doi.org/10.1016/S0140-7007(00)00039-6.
[25] Matches software; 2016. Retrieved from http://www.matche.com/equipcost/Default.html.
[26] Brooke A, Kendrick D, Meeraus A. GAMS e a user's guide (release 2.25). San Francisco (CA): The Scientific Press; 1996.
[27] Drud AS. CONOPT, a GRG code for large scale non linear optimization. reference manual. Bagsvaerd (Denmark): ARKI Consulting and Development A/S; 1992.
[28] Druetta P, Aguirre P, Mussati S. Minimizing the total cost of multi effect evaporation systems for seawater desalination. Desalination 2014;344:431–45. http://dx.doi.org/10.1016/j.desal.2014.04.00. ISSN: 0011-9164 Elsevier B.V. Ltd.
[29] Druetta P, Aguirre P, Mussati S. Optimization of multi-effect evaporation desalination plants. Desalination 2013;331:1–15. http://dx.doi.org/10.1016/j.desal.2012.10.03. ISSN: 0011-9164 Elsevier B.V. Ltd.
[30] Alasino N, Mussati MC, Scenna N. Wastewater treatment plant synthesis and design. Ind Eng Chem Res 2007;46:7497–512. http://dx.doi.org/10.1021/ie0704905.
[31] Alasino N, Mussati MC, Scenna NJ, Aguirre P. Wastewater treatment plant synthesis and design: combined biological nitrogen and phosphorus removal. Ind Eng Chem Res 2010;49:8601–12. http://dx.doi.org/10.1021/ie1000482.
[32] Mussati MC, Aguirre PA, Espinosa J, Iribarren OA. Optimal design of azeotropic batch distillation. AIChE J 2006;52:968–85. http://dx.doi.org/10.1002/aic.10696.
[33] Oliva DG, Francesconi JA, Mussati MC, Aguirre PA. Modeling, synthesis and optimization of heat exchanger networks. Application to fuel processing systems for PEM fuel cells. Int J Hydrogen Energy 2011;36:9098–114. http://dx.doi.org/10.1016/j.ijhydene.2011.04.097.
[34] Manassaldi J, Mores P, Scenna N, Mussati SF. Optimal design and operating conditions of an integrated plant using a natural gas combined cycle and

postcombustion CO_2 capture. Ind Eng Chem Res 2014;53:17026–42. http://dx.doi.org/10.1021/ie500463.
[35] Mores P, Godoy E, Mussati S, Scenna N. A NGCC power plant with a CO_2 post-combustion capture option. Optimal economics for different generation/capture goals. Chem Eng Res Des 2014;92:1329–53. http://dx.doi.org/10.1016/j.cherd.2013.11.01.
[36] Arias AM, Mores P, Scenna N, Mussati S. Optimal design and sensitivity analysis of post-combustion CO_2 capture process by chemical absorption with amines. J Clean Prod 2016;115:315–31. http://dx.doi.org/10.1016/j.jclepro.2015.12.056.
[37] Mores P, Scenna N, Mussati S. CO_2 capture using MEA aqueous solution: modeling and optimization of the solvent regeneration and CO_2 desorption process. Energy 2012;45(1):1042–58. http://dx.doi.org/10.1016/j.energy.2012.06.03.
[38] Arias AM, Mussati MC, Mores PL, Scenna NJ, Caballero JA, Mussati SF. Optimization of multi-stage membrane systems for CO_2 capture from flue gas. Int J Greenhouse Gas Control 2016;53:371–90. http://dx.doi.org/10.1016/j.ijggc.2016.08.005.
[39] Bisschop J, Entriken R. AIMMS – the modeling system. Haarlem (The Netherlands): Paragon Decision Technology; 1993.
[40] Fourer R, Gay DM, Kernighan BW. AMPL – a modeling language for mathematical programming. Redwood City (CA): The Scientific Press; 1993.
[41] Holmstrom K. The TOMLAB optimization environment in matlab. Adv Model Opt 1999;1(1):47–69.
[42] . LINGO – the modeling language and optimizer. Chicago (IL): LINDO Systems Inc.; 1995.
[43] Piela PC, Epperly TG, Westerberg KM, Westerberg AW. ASCEND: an object-oriented computer environment for modeling and analysis: the modeling language. Comp Chem Eng 1991;15:53–72. http://dx.doi.org/10.1016/0098-1354(91)87006-U.
[44] LANCELOT: a Fortran package for large-scale nonlinear optimization (release A). Springer series in computational mathematics, 17. New York: Springer-Verlag; 1992.
[45] Dash Optimization. XPRESS-MP; 2001. www.dash.co.uk/.
[46] Dinçer İ, Zamfirescu C. Sustainable energy systems and applications. Boston (MA, USA): Springer; 2012.